Journal of Molecular Structure 1265 (2022) 133358

Contents lists available at ScienceDirect

Journal of Molecular Structure

journal homepage: www.elsevier.com/locate/molstr

Exploration of supramolecular and theoretical aspects of two new Cu(II) complexes: On the importance of lone pair···π(chelate ring) and π···π(chelate ring) interactions

Samit Pramanik[a], Sudipta Pathak[b], Antonio Frontera[c,*], Subrata Mukhopadhyay[a,*]

[a] Department of Chemistry, Jadavpur University, Kolkata 700032, India
[b] Department of Chemistry, Haldia Government College, Debhog, Purba Medinipur 721657, West Bengal, India
[c] Departament de Química, Universitat de les Illes Balears, Crta. de Valldemossa km 7.5, 07122 Palma de Mallorca (Baleares), Spain

ARTICLE INFO

Article history:
Received 28 March 2022
Revised 14 May 2022
Accepted 22 May 2022
Available online 23 May 2022

Keywords:
Copper(II) complexes
X-ray crystal structures
Non-covalent interactions
DFT calculation

ABSTRACT

An organic ligand, **NL** [4-(1-methylimidazole)-2,6-di(pyrazinyl)pyridine] has been synthesized and characterized by several spectroscopic methods. The ligand (**NL**) was then utilized for the preparation of two complexes, namely, [Cu(**NL**)(N_3)(H_2O)]ClO_4·H_2O (complex **1**) and {[Cu(**NL**)(μ-**NL**)NCS]ClO_4}$_n$ (complex **2**). The crystal structures of these complexes have been established by single-crystal X-ray analysis. Complex **2** exhibits a one dimensional (1-D) polymeric chain, whereas complex **1** is a mononuclear one. It is noteworthy that the change in auxiliary ligands exhibit structural variations and different supramolecular behaviors for the present complexes. Mainly, lone pair···π(chelate ring) and π···π(chelate ring) interactions are well investigated in governing the solid state architecture of complex **1** and **2** respectively. Besides, the other non-covalent interactions like π···π stacking, sulphur (lone pair)···π and hydrogen bonding interactions play crucial role in the crystal packing for both the complexes. In complex **1**, a chair-like perchlorate–water tetrameric cluster, $[(ClO_4)_2–(H_2O)_2]^{2-}$was observed. The aim of this work is to investigate the role of chelate rings in producing supramolecular architectures of both the complexes in the solid state. Theoretical (DFT) calculations including QTAIM and NCI Plot index were carried out to analyze the non-covalent interactions in the solid state for both the complexes.

1. Introduction

Supramolecular chemistry deals with the design, synthesis and self-assembly of well-defined molecular components into tailor-made architectures by using intermolecular interactions [1–3]. Crystal engineers always help to study various intermolecular interactions in the journey from molecule to crystal in the solid state [4–7]. Over the last few years, crystal engineering has matured enough and interplayed between structure and properties of molecules in a programmed way [8–10]. However, finding of new interactions by creative and intellectual way in designing and building crystal architecture is one keen interest in crystal engineering.

Hydrogen bonding has been extensively well studied as it universally exists in both natural and artificial substances [11,12]. Not only hydrogen bonds but also other dispersive interactions like π···π stacking, anion···π and lone pair···π interactions play a decisive role in nucleation and growth of molecular crystals in recent years [13–21]. Among those, lone pair···π interaction is a significant binding mode which plays a key role in stabilizing the structures of nucleic acids and modulating the recognition of protein DNA and enzyme substrates [22–24]. Recently, the attention has shifted toward more unconventional interactions such as π(arene)···π(chelate ring), π(chelate ring)···π(chelate ring), lone pair···π(chelate ring), C–H···π(chelate ring), etc. interactions which have been proven to have equal or even dominating contributions to molecular crystal formation [25–34]. Chelate rings are recognized to exhibit metallo-aromatic behavior and undoubtedly they can take part in similar interactions to their organic counterparts [35,36]. In the context of supramolecular architecture of coordination compounds, contribution of chelate ring (formed by metal coordination using heterocyclic π-systems) assisted interactions have arrested recent interest of researchers.

As an NNN-tridentate ligand, terpyridine plays an important role in supramolecular chemistry as well in coordination chemistry due to its π stacking ability among themselves and excel-

* Corresponding authors.
E-mail address: toni.frontera@uib.es (A. Frontera).

https://doi.org/10.1016/j.molstruc.2022.133358

lent chelating capability with various metal cations [37]. Terpyridine or their structural analogs show very high binding potentiality towards transition metal ions due to *cis, cis* arrangement of the three nitrogen atoms and $d\pi-p\pi^*$ back bonding of the metal to pyridine rings [38]. However, they always prefer to adopt a planar geometry to achieve maximum conjugation in the complexes [39]. Terpyridine metal complexes have been synthesized and developed rapidly for their potential applications in several fields, for instance, photovoltaic devices [40,41], DNA bindings [42,43], sensors [44,45], photo-sensitizers [46,47], catalysis [48,49], metal-organic framework (MOF) construction [50,51], and many more [52]. Recently, increasing attention has been paid to the synthesis of 4′-substituted terpyridine complexes with potential applications in accessing new classes of functional materials possessing photo-physical and electrochemical properties [53–56]. As terpyridines are generally neutral during complex formation, ancillary ligands like pseudo halides (azido, thiocyanato, etc.) are often employed to sustain electrical neutrality. Azido (N_3^-) and thiocyanato (SCN^-) pseudo halide ions have also been extensively used as bridging ligands in the construction of coordination compounds due to their diversity of bonding modes with 3d metal complexes [57–62]. As a terminal ligand, the coordination mode of SCN^- depends on the electronic nature and oxidation state of the metal ion [63]. Besides, other factors like steric effect, type of solvent, non-coordinated ions and even electronic nature of the auxiliary ligands can influence the coordination mode of the thiocyanato ligand, particularly when the metal ion has intermediate hard–soft acid character [64]. Azido and thiocyanato copper(II) complexes with trigonal bipyramidal (TBP) or square pyramidal (SP) geometry have already gained much attention for the last few years but, there still remains much more work to be explored. Among the investigated metals, Cu(II) containing complexes have received increasing attention due to their promising applications in various fields such as catalysis, energy harvesting devices, medicinal chemistry and in related areas in the recent past [65–72]. After iron and zinc, copper is the third most abundant transition metal in the human body and plays an important role in hemopoiesis, metabolism, growth and immune system [73,74]. Most importantly, the reversible change of the oxidation state of Cu(I)/Cu(II) couple under physiological conditions has promoted the development of metal complexes with an active redox chemistry within cancerous cells [75,76]. Besides, compared to other common metal ions, Cu(II) ion exhibits high binding constant with various ligands in chemical and biological systems [77,78]. Keeping all these factors in mind, two new Cu(II) complexes have been synthesized based on 4-(1-methylimidazole)-2,6-di(pyrazinyl)pyridine (**NL**) with auxiliary ligands azido (for complex **1**) and thiocyanato (for complex **2**) in aqueous medium (Scheme S1). Both the complexes adopt distorted square pyramidal (SP) geometry where the title ligand, (**NL**) acts as an NNN-tridentate ligand. In both the complexes, the ligand (**NL**) coordinates the Cu(II) ion through three coplanar ligating sites involving one pyridyl nitrogen atom (N3) and two pyrazinyl nitrogen atoms (N5 and N6) forming two five-membered chelate rings (Scheme S1). The metallo-aromatic nature of the chelate rings gives rise to the possibility of alternative π-systems which play an important role in producing various supramolecular architectures for both the complexes in the solid state. Interestingly, a dimer is shaped by two symmetrically equivalent lone pair$\cdots\pi$(chelate ring) interactions between lone pair on azide nitrogen atom (N8) and Cg(2) chelate ring in complex **1**. From the structural database survey, it is evident that the lone pair$\cdots\pi$(chelate ring) interactions involving halogen atoms (Cl, Br, I) are common but to the best of our knowledge the engagement of pnictogen atom like nitrogen in lone pair$\cdots\pi$(chelate ring) interaction is comparatively less familiar [127–131]. In complex **1**, the perchlorate anion is involved in the formation of a tetrameric anion–water cluster, $[(ClO_4)_2{-}(H_2O)_2]^{2-}$, which is less frequent. To our knowledge, a few perchlorate–water tetrameric clusters have been characterized in the solid state [79–81]. For complex **2**, the influence of $\pi\cdots\pi$(chelate ring) and sulphur(lone pair)$\cdots\pi$ interactions have been well established in the crystal packing. Finally, the present work utilizes DFT calculations and several computational tools (QTAIM and NCI Plot) to analyze the noncovalent interactions focusing on lone pair$\cdots\pi$(chelate ring) and $\pi\cdots\pi$(chelate ring) interactions in stabilizing the solid state architectures of both the complexes. We have also evaluated energetically how the presence of the perchlorate–water cluster influences the crystal packing of complex **1** in the solid state.

2. Experimental sections

2.1. Materials and apparatus

All the chemical reagents (analytical grade) and solvents (spectroscopic grade) were purchased from commercial suppliers and used without any further purification. Freshly boiled double distilled water was used throughout the synthetic procedure and all the reactions were carried out under aerobic conditions. Elemental analyses (C, H and N) were performed using a PerkinElmer 2400 Series-II CHN analyzer, USA, elemental analyzer. ESI mass spectra were obtained from a Water HRMS model XEVO-G2QTOF#YCA351 spectrometer. ^{1}H NMR and ^{13}C NMR spectra were obtained from Bruker spectrometer (300 MHz) with $CDCl_3$ solvent using trimethylsilane (TMS) as an internal standard. Fourier transform infrared (FT-IR) spectra were recorded on a Perkin Elmer LX-1 FT-IR spectrophotometer (4000–400 cm^{-1}) by using a modern diamond attenuated total reflectance (ATR) accessory method.

2.2. Syntheses

2.2.1. Synthesis of 4-(1-methylimidazole)-2,6-di(pyrazinyl)pyridine [NL]

Acetylpyrazine (0.305 g, 2.5 mmol) was added into 30 mL ethanolic solution of 1-methyl imidazole-2-carboxaldehyde (0.11 g, 1 mmol). 3 mL of 1 (M) aqueous solution of NaOH was added drop wise into the reaction mixture at room temperature (Scheme 1). Then 5 mL aqueous NH_3 (35%) solution was discharged into the basic solution at a time. The reaction mixture was then refluxed for 3 h. After completion of the reaction, solution was cooled at room temperature. A light-yellow solid formed which was collected by filtration and washed repeatedly with coldwater and dried in air. The desired product was obtained with good yield and acceptable purity, Yield 0.214 g (68%). Anal. calc. for $C_{17}H_{13}N_7$, C 64.75, H 4.16, N 31.09. Found: C 64.12, H 3.89, N 30.79%. ^{1}H NMR (300 MHz, $CDCl_3$): δ (ppm) = 9.85 (s, 2H), 8.83 (s, 2H), 8.65 (s, 4H), 7.24 (s, 1H), 7.09 (s, 1H), 3.99 (s, 3H) (Fig. S1). ^{13}C NMR (75 MHz, $CDCl_3$): δ (ppm) =154.50, 150.46, 144.93, 143.70, 143.48, 140.37, 129.60, 124.24, 120.55, 35.17 (Fig. S2). Main FT-IR absorptions, (KBr, cm^{-1}): 1980(s), 1606(vs), 1570(vs), 1519(s), 1464(s), 1456(s), 1419(s), 1371(vs), 1292(s), 1257(s), 1224(s), 1120(vs) (Fig. S3). ESI-MS: *m/z* 316.12, calcd. for $[C_{17}H_{13}N_7 + H]^+$ 316.13 (Fig. S4).

2.2.2. Synthesis of [Cu(NL)(N$_3$)(OH$_2$)]ClO$_4$·H$_2$O(complex 1)

An aqueous suspension (15 mL) of the ligand, **NL** (0.0315 g, 0.1 mmol) was added drop wise to 15 mL of aqueous $Cu(ClO_4)_2{\cdot}6H_2O$ (0.0370 g, 0.1 mmol) solution with constant stirring. An aqueous solution (5 mL) of NaN_3 (0.0065 g, 0.1 mmol) was added and stirred for 3 h (Scheme 2). Then the solution was filtered and the filtrate was left for slow evaporation without any disturbance. After one-week, deep green X-ray quality crystals of **1** were isolated (yield: 68%). Solubility of the complex was checked in some common solvents for further applications and found to

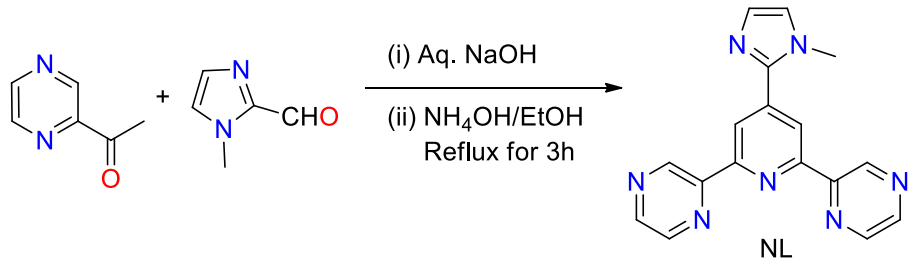

Scheme 1. Synthetic route for the ligand, **NL**.

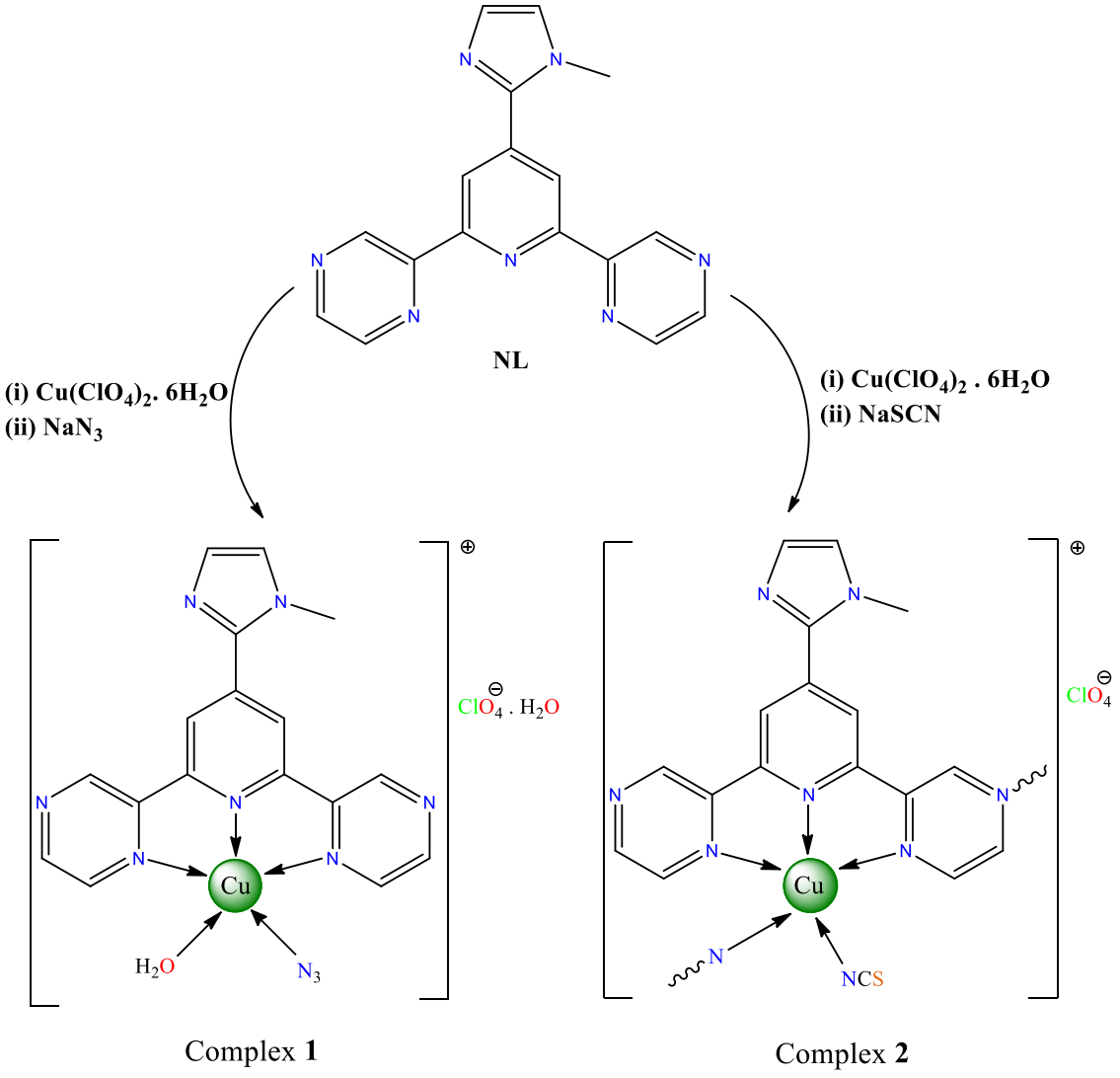

Scheme 2. Schematic representations of the synthesis of complex **1** and **2**.

be insoluble in water and methanol whereas completely soluble in acetonitrile, DMSO and DMF. Anal. calc. for $C_{17}H_{17}CuN_{10}ClO_6$: C, 36.70; H, 3.08; N, 25.17. Found: C, 36.63; H, 2.99; N, 25.13%. Main FT-IR absorptions, (KBr, cm^{-1}): 3543(w), 3469(s), 3229(w), 3139(vs), 3102(s), 2050(vs), 1614(vs), 1590(s), 1557(s), 1496(s), 1470(vs), 1433(s), 1408(s), 1340(s), 1299(s), 1283(s), 1227(s) (Fig. S5).

2.2.3. Synthesis of {[Cu(NL)(μ-NL)NCS]ClO_4}$_n$ (complex 2)

An aqueous suspension (15 mL) of the ligand, **NL** (0.0315 g, 0.1 mmol) was added drop wise to 15 mL aqueous $Cu(ClO_4)_2{\cdot}6H_2O$ (0.0370 g, 0.1 mmol) solution at stirring condition. An aqueous solution (5 mL) of NaSCN (0.0081 g, 0.1 mmol) was added and stirred for 4 h (Scheme 2). Then the solution was filtered and the filtrate was left undisturbed for slow evaporation. Two weeks later, deep brown X-ray quality crystals of **2** were obtained (yield: 63%). The complex **2** was insoluble in water and methanol, partly soluble in acetonitrile and completely soluble in DMSO as well as in DMF. Anal. calc. for $C_{18}H_{13}CuN_8SClO_4$: C, 40.30; H, 2.44; N, 20.89. Found: C, 40.25; H, 2.39; N, 20.85%. Main FT-IR absorptions, (KBr, cm^{-1}): 3218(s), 3114(bs), 2100(vs), 2047(vs), 1611(s), 1599(s), 1554(s), 1497(s), 1470(s), 1423(s), 1406(s), 1332(vs), 1298(s), 1288(s), 1225(s) (Fig. S6).

(Caution! Salts of perchlorate and azide are potentially explosive. Only small amounts of materials should be prepared and to be handled with extreme care).

2.3. X-ray crystallography analysis

Single crystal X-ray data were collected by using a Bruker SMART APEX II CCD area detector equipped with a graphite monochromated Mo Ka radiation (λ = 0.71073 Å) source in φ and ω scan mode at 296 K for both the complexes. Cell parameter refinement and data reduction for both the complexes were carried out using a Bruker SMART APEX II instrument and Bruker SAINT Software [82]. The crystal structures of both the complexes were solved by SHELXT-2014/5 and refined by full-matrix least squares on F^2 techniques using the SHELXL-2016/6 crystallographic software package [83,84]. The CIFs have been deposited with CCDC No. 2096470 (complex **1**) and CCDC No. 2096471 (complex **2**). Selected crystal structure refinement parameters for **1** and **2** are given in Table S1. The important bond lengths and bond angles are included in Tables S2 and S3, respectively for the title complexes.

2.4. Computational methods

The non-covalent interactions were analysed energetically using Gaussian-16 [85] at the PBE0-D3/def2-TZVP level of theory. The binding energies have been corrected using the Boys and Bernardi counterpoise method [86]. The Grimme's D3 dispersion correction has been also used in the calculations [87]. To evaluate the interactions in the solid state, the crystallographic coordinates were used and only the position of the hydrogen bonds has been optimized. This methodology [88,89] and level of theory [90–100] (functional and basis set) have been previously used to analyze non-covalent interactions in the solid state. The interaction energies were estimated by calculating the difference between the energies of the isolated monomers and the ones of their assembly. For the calculations, the monomeric Cu(II) species were considered as doublets (one unpaired electron) and the dimers as triplets (two unpaired alpha electrons). The NCI plot [101] isosurfaces have been used to characterize non-covalent interactions. They correspond to both favorable and unfavorable interactions, as differentiated by the sign of the second density Hessian Eigen value and defined by the isosurface color. The color scheme is a red-yellow-green-blue scale with red for ρ^{+}_{cut} (repulsive) and blue for ρ^{-}_{cut} (attractive).

3. Results and discussion

3.1. Synthesis and IR spectroscopic characterization

The copper(II) complexes **1** and **2** were prepared by using newly synthesized 4-(1-methylimidazole)-2,6-di(pyrazinyl)pyridine [**NL**] moiety as the main ligand with different auxiliary ligands (azide anion for **1** and thiocyanato anion for **2**) at room temperature in aqueous medium (Scheme 2). Strategically 1:1:1 molar ratio was maintained to synthesize the mixed ligand complexes (to avoid bis-terpyridine complexes) having product stoichiometry Cu(II): **NL**: N_3^- = 1:1:1 for complex **1** and Cu(II): **NL**: SCN^- = 1:1:1 for complex **2**. Interestingly, when sodium azide (NaN_3) was used as the auxiliary ligand in combination with the **NL** ligand, the formation of the mononuclear complex **1** was observed, while similar reaction condition with sodium thiocyanate (NaSCN) results in the 1D coordination polymeric complex **2**. Both the complexes were isolated as air stable green colored crystalline solids in good yields (68% for **1** and 63% for **2**). Hence, the synthesis presented herein composed of copper(II) perchlorate as a metal source and **NL** as a primary ligand, together with easily accessible and cheap auxiliary ligands ($N_3^-$and SCN^-) in a simple one-pot synthetic procedure for engineering of diverse metal-organic assemblies in organic-solvent-free medium.

The molecular structures of the title complexes have been established by single crystal X-ray analysis and supported by IR spectroscopy. The IR spectrum of complex **1** shows typical ν(OH) vibrations in the 3543−3229 cm^{-1} range for both coordinated and non-coordinated water molecules. Besides, the complex **1** displays a very sharp $\nu_{as}(N_3)$ band with maximum at 2050 cm^{-1}, while that at 1340 cm^{-1} is presumably associated with the $\nu_s(N_3)$ vibration. The presence of auxiliary NCS ligand in complex **2** is confirmed with the detection of a very intense ν_{as}(CN) band at 2047 cm^{-1} with a shoulder at 2100 cm^{-1}, which are typical for the terminal N-bonded isothiocyanate moieties [57,102–105]. In addition, the ν(CH) vibrations are detected in the range of 3218−3102 cm^{-1} for both the complexes. The observed stretching frequencies for $\nu_{as}(N_3)$ and ν_{as}(CN) in our complexes (**1** and **2**) are in good agreement with some reported Cu(II) complexes which are summarized in Table S4.

3.2. Structural description of complex 1

The asymmetric unit of complex **1** with the atom numbering scheme is shown in Fig. 1. The formula unit of complex **1** shows one monomeric cationic $[Cu(C_{17}H_{13}N_7)(N_3)(H_2O)]^+$ unit, one non-coordinated perchlorate anion and one non-coordinated water molecule. The complex crystallizes in a triclinic system with the space group $P\bar{1}$ and its unit cell contains two formula units. The coordination mode around the metal center can be best described as a distorted square pyramid [τ value [106] is 0.0213 (ideally 0 for perfect square pyramidal geometry and 1 for trigonal bipyramidal geometry), eq S1] where the equatorial plane is shaped by the three pyrazinyl nitrogen atoms (N3,

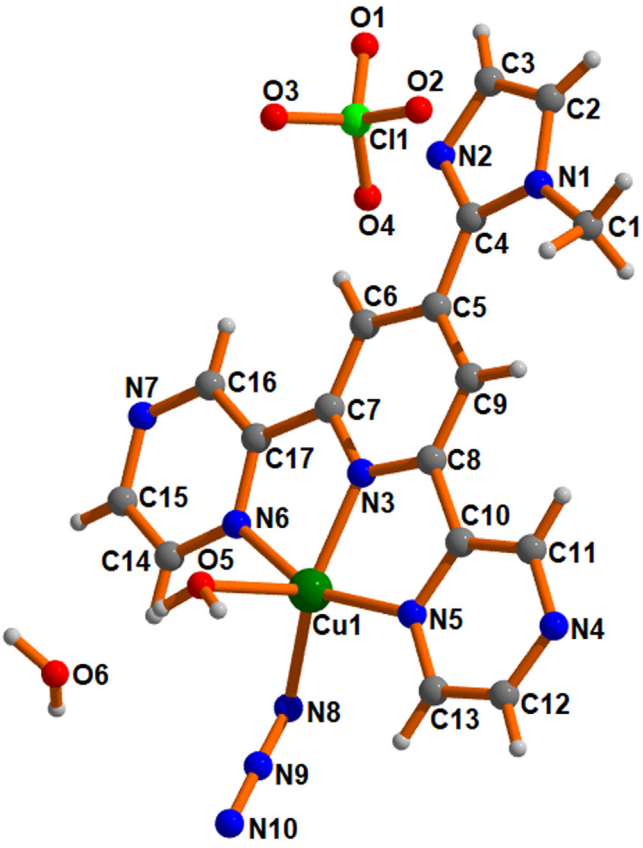

Fig. 1. Asymmetric unit of complex **1**.

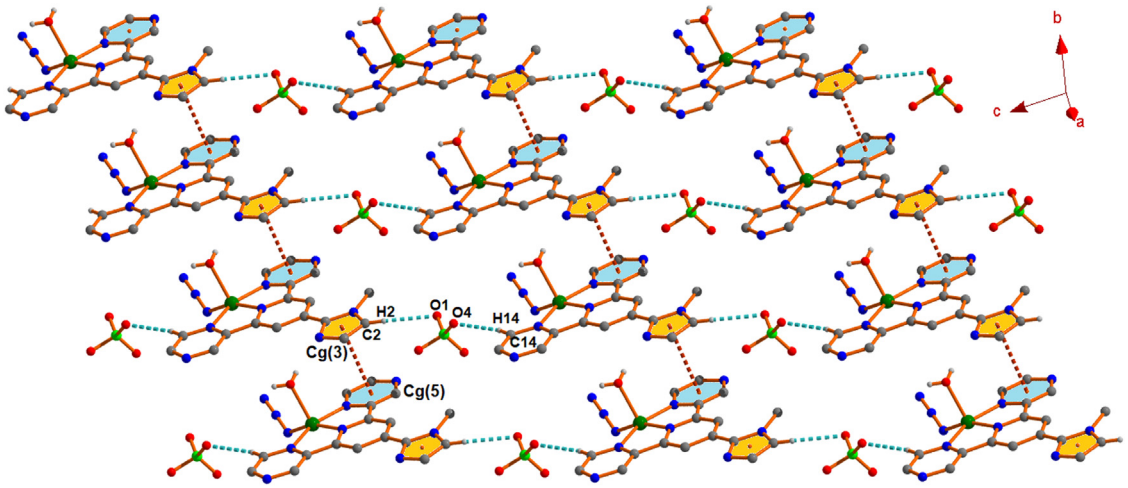

Fig. 2. Perspective view of the formation of a 2-D architecture through $\pi\cdots\pi$ stacking and C–H···O hydrogen bonding interactions in complex **1**.

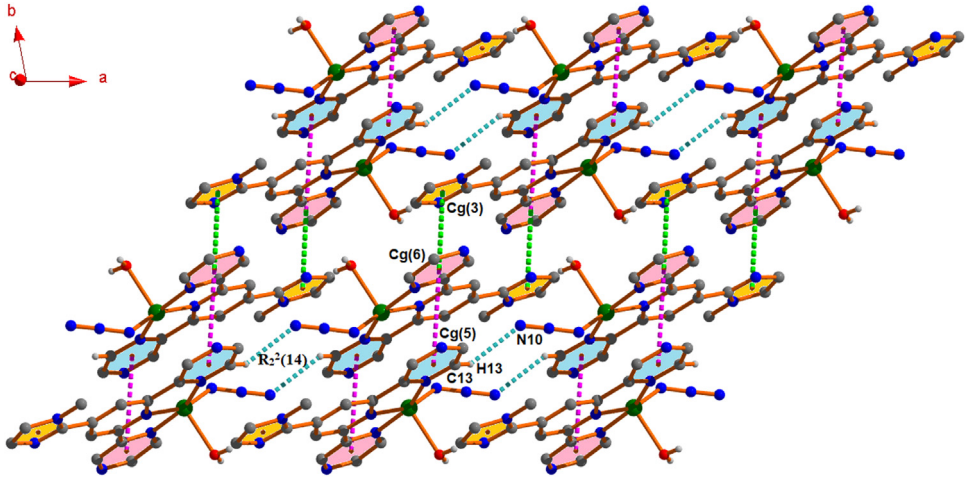

Fig. 3. Perspective view of 2-D supramolecular network through $\pi\cdots\pi$ stacking and C–H···N hydrogen bonding interactions in complex **1**.

N5 and N6) of the ligand (**NL)** and one nitrogen atom (N8) of azide anion. The apical position is occupied by one oxygen atom (O5) of a water molecule. Here the ligand (**NL**) is able to bind the Cu(II) ion to produce two five-membered chelate rings, (Cu1/N3/C7/C17/N6) and (Cu1/N3/C8/C10/N5) having bite angles [N3–Cu1–N6 = 79.28(9)° and N3–Cu1–N5 = 79.42(8)°] respectively. The average distance of Cu–N bonds in the equatorial plane is 1.988 Å [Cu1–N5 = 2.042(2) Å, Cu1–N6 = 2.044(2) Å, Cu1–N3 = 1.9431(19) Å and Cu1–N8 = 1.923(3) Å]. The axial Cu–O bond is comparatively longer [Cu1–O5 = 2.224(2) Å] than the equatorial Cu–N bonds and is expected as the axial bond utilizes more 'p' character of the orbital in forming the bond, which makes the axially coordinated water oxygen atom more electronegative [107]. The Cu(II) ion is deviated by a distance of 0.259 Å towards the axial water oxygen atom (O5) from the equatorial plane (N3, N5, N6 and N8). The dipositive charge on the metal center is stabilized by one coordinated azide anion and one non-coordinated perchlorate anion.

The solid-state structure of complex **1** is stabilized through the combination of C–H···N, C–H···O, O–H···N, O–H···O hydrogen bonds along with $\pi\cdots\pi$ stacking and lone pair$\cdots\pi$ (chelate ring) interactions (Table S5 and S6). In the first architecture (Fig. 2), the monomeric unit of complex **1** propagates to produce a 1-D polymeric chain through a $\pi\cdots\pi$ interaction (Table S6) between Cg(3) of one unit with Cg(5) of the other unit with a ring separation distance of 3.4928(19) Å. Now, perchlorate ions connect these parallel 1-D chains through C2–H2···O1 (169°) and C14–H14···O4 (154°) hydrogen bonding interactions at (-x, 1-y, 2-z) and (1-x, 1-y, 1-z) respectively; thus leading to the formation of a 2-D architecture in the *bc*-plane.

A different 2-D layer is generated through $\pi\cdots\pi$ stacking and C–H···N hydrogen bonding interactions (Fig. 3) for complex **1**. The self-complementary nature leads the molecules to form a dimer through $\pi\cdots\pi$ interaction between Cg(5) and Cg(6) of two different units. The inter-planar spacing between Cg(5) and Cg(6) is 3.8956(18) Å. Interconnection of the dimers through another self-complementary Cg(3)–Cg(6) interaction ($\pi\cdots\pi$ stacking) which leads to form an infinite chain along the [010] direction. The separation distance between Cg(3) and Cg(6) is 3.642(2) Å. Due to the self-complementary nature, the parallel chains are again interlinked through weak C13–H13···N10 hydrogen bond by generating a $R_2^2(14)$ ring motif. Here, the aromatic fragment (C13–H13) of one unit acts as donor to the azide nitrogen atom (N10) of adjacent unit at (2-x, 2-y, 1-z) with an angle of 130° All these interactions are cumulatively associated to extrapolate the dimensionality from 1-D to 2-D in the *ab*-plane (as shown in Fig. 3).

A comprehensive analysis exhibits a dimeric distribution (shown in Fig. 4) that is formed by two symmetrically equivalent lone pair$\cdots\pi$(chelate ring) interaction in complex **1**. Here, two monomeric units are arranged almost in opposite orienta-

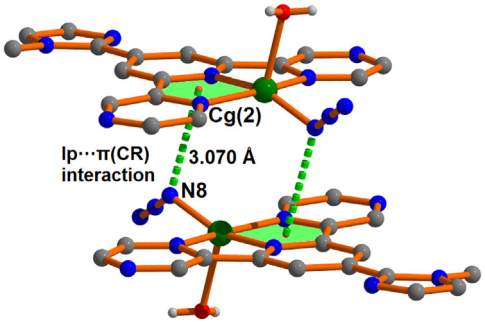

Fig. 4. Dimeric distribution in complex **1** through lone pair···π(chelate ring) interactions.

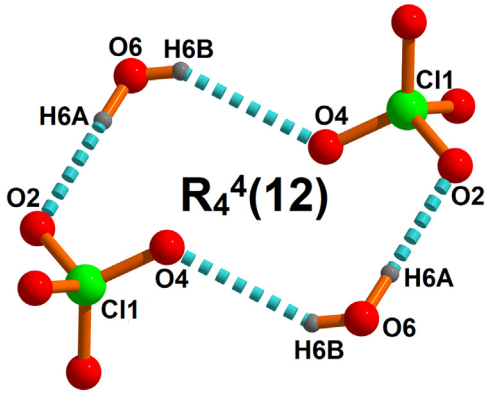

Fig. 5. Formation of anion–water cluster by strong O–H···O hydrogen bonding interactions in complex **1**.

tion one above the other to achieve a self complementary lone pair···π(chelate ring) interaction between lone pair on azide nitrogen atom (N8) and Cg(2) chelate ring (Cu1/N3/C8/C10/N5) having a shortest separation distance of 3.070 Å. The Cu···Cu separation in this dimeric integrity is 3.917 Å which suggests that there may be some type of weak metal···metal interaction to stabilize this dimeric form [108].

The solvent water molecules not only tie up themselves for the formation of clusters but also suitable anions participate in the assembly process to satisfy donor–acceptor balance and thus construct anion–water clusters [109,110]. It is worth mentioning that, the behavior of hydrated anion is quite different from that of bare anion or anion in nonpolar media. Thus, studies of anion–water clusters are vitally important in understanding the hydration phenomena of both organic and inorganic anions in nature as well as in biochemistry. In complex **1**, a chair-like perchlorate–water tetrameric cluster, $[(ClO_4)_2{-}(H_2O)_2]^{2-}$, is decorated due to the self-complementary nature of intermolecular hydrogen bonding interactions between two free water molecules and two perchlorate anions (as depicted in Fig. 5). Here, the non-coordinated water oxygen atom O(6) acts as double donor to the oxygen atoms O(2) and O(4) of perchlorate ion in the complex at (169°) and (153°) respectively; thus forming a $R_4^4(12)$ ring motif (Table S5). It was well established that the lower H···A separation and the D–H···A angle close to 180° indicate the stronger hydrogen bonding interaction. Here, the O6–H6A···O2 interaction is relatively stronger than that of O6–H6B···O4 interaction as the former interaction has lower H···O distance (2.0 Å) compared to other (2.23 Å) and O–H···O angle close to 180°. The O···O separation distances within the tetramer in the range of 2.839(6)–3.006(8) Å, which is longer than the value in ice I_c (2.75 Å) and ice I_h (2.759 Å), but can be compared with the corresponding values observed in liquid water (2.854 Å) [111,112]. Interestingly, the perchlorate–water cluster helps in growth of the molecular crystal by filling the void spaces present in complex **1** (as shown in Fig. 6). We have studied the mutual influence of the hydrogen bonding interactions in the perchlorate–water cluster by means of QTAIM analysis (shown in Fig. 16).

The lone pair···π(chelate ring) along with $\pi\cdots\pi$ stacking and hydrogen bonding interactions play a decisive role in building the supramolecular arrangement (Fig. 6). The dimeric units (as de-

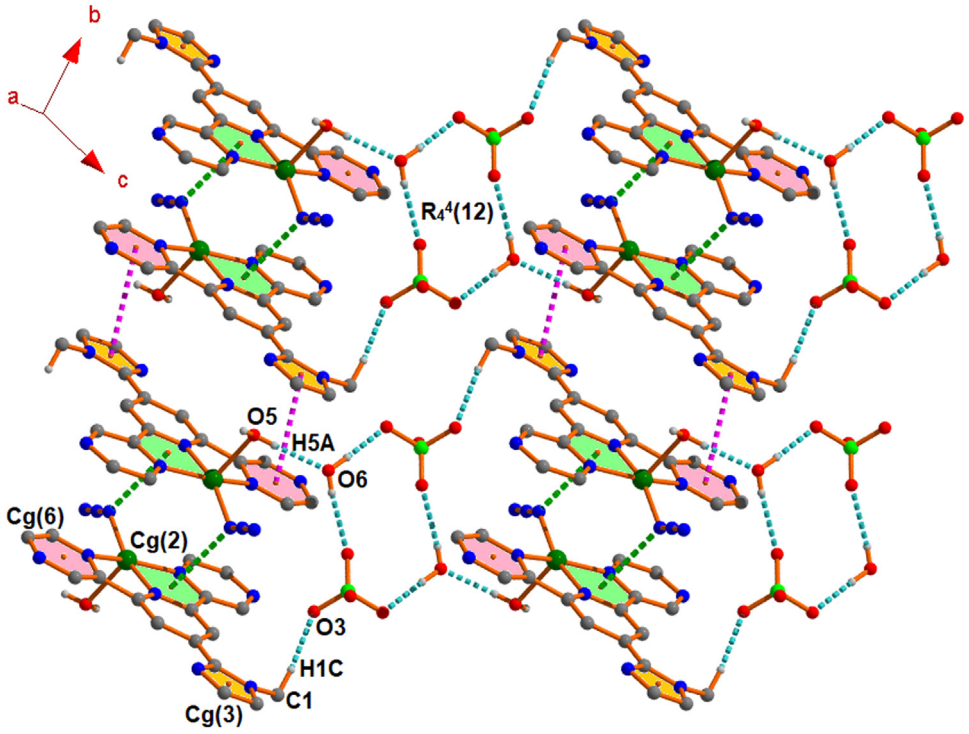

Fig. 6. Perspective view of 2-D arrangement incorporating $\pi\cdots\pi$, lone pair···π(chelate ring) and hydrogen bonding interactions in complex **1**.

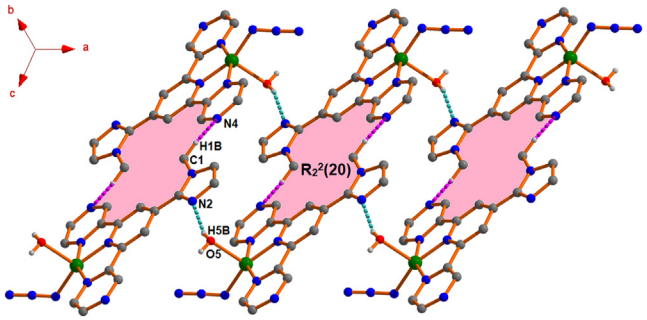

Fig. 7. Formation of 1-D tape by hydrogen bonding interactions in complex **1**.

picted in Fig. 4) are interlinked by a self complementary $\pi\cdots\pi$ interaction between Cg(3) and Cg(6) of two different units leading the formation of a 1-D chain along [010] direction. The separation distance between Cg(3) and Cg(6) ring centriods is 3.642(2) Å (Table S6). Now, these 1-D parallel chains are further connected by the anion–water cluster (shown in Fig. 5) to generate the 2-D arrangement in the *bc*-plane. Here, the water-anion clusters are interconnected with the dimeric units by the self complementary strong O5–H5A···O6 (175°) and comparatively weak C1–H1C···O3 (158°) hydrogen bonding interactions (Table S5) as shown in Fig. 6.

Two monomeric units of complex **1** are interconnected by the self complementary C1–H1B···N4 (133°) hydrogen bonding interactions (Table S5) to form another dimer having $R_2^2(20)$ ring motif (Fig. 7). The dimeric units are further interlinked through the self complementary O5–H5A···N2 [165(5)°] hydrogen bonding interactions where coordinated water oxygen atom (O5) acts as donor to the imidazole nitrogen atom (N2) in the molecule at (1 + *x*, y, z). Repetition of this $R_2^2(20)$ ring motif along [100] direction leads the molecules to generate a 1-D tape as shown in Fig. 7.

3.3. Structural description of complex 2

The complex **2** is a coordination polymer (Fig. 8) and the asymmetric unit of the complex with the atom numbering scheme is depicted in Fig. 8. In this polymeric chain the asymmetric units are connected along the (010) direction through pyrazine nitrogen atom (N4) of the second ligand (**NL**). Single-crystal X-ray diffraction study shows that the complex **2** adopts a monoclinic system with the space group $P2_1/c$ and its unit cell contains four formula units. In the complex, the central Cu(II) ion is situated in a distorted square pyramidal geometry (τ = 0.1218, eq S1) where the equatorial plane is formed by the three pyrazinyl nitrogen atoms (N3, N5 and N6) of the ligand (**NL**) and one nitrogen atom (N8) of thiocyanate anion. The apical position is occupied by another nitrogen atom (N4)

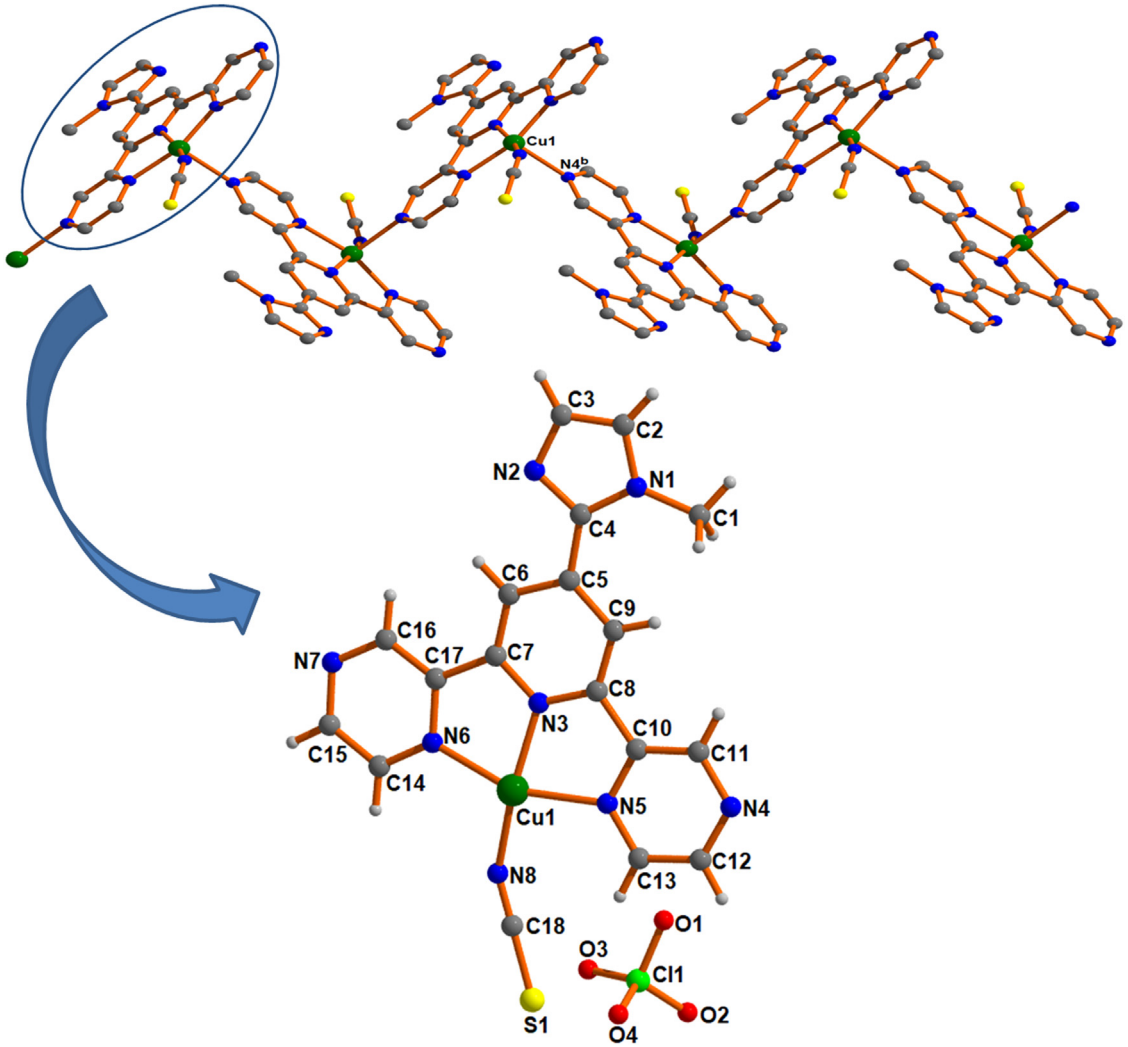

Fig. 8. One-dimensional (1-D) zigzag polymeric chain along the [010] direction and the asymmetric unit of complex **2**.

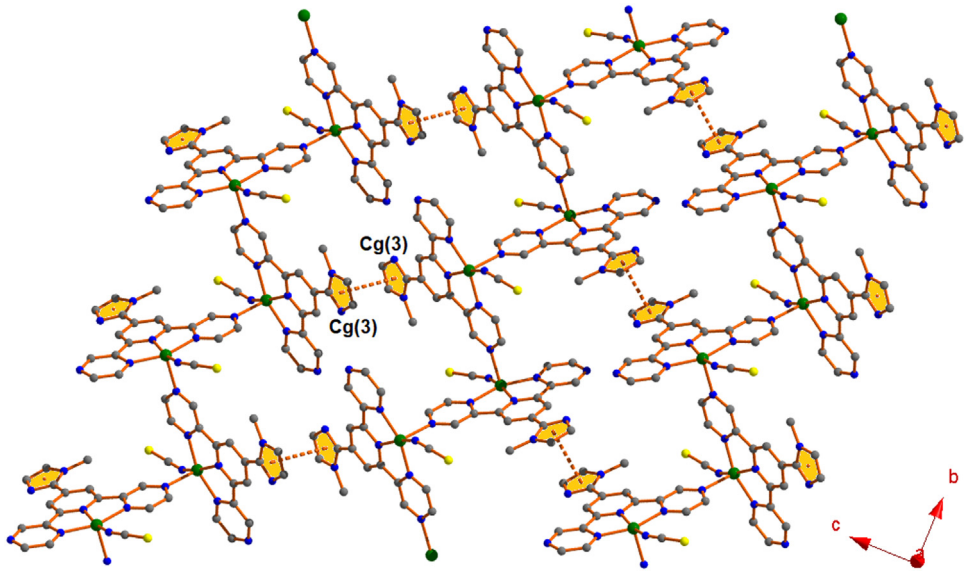

Fig. 9. Perspective view of 2-D layer generated through $\pi\cdots\pi$ interactions in complex **2** (aromatic hydrogen atoms have been omitted for clarity).

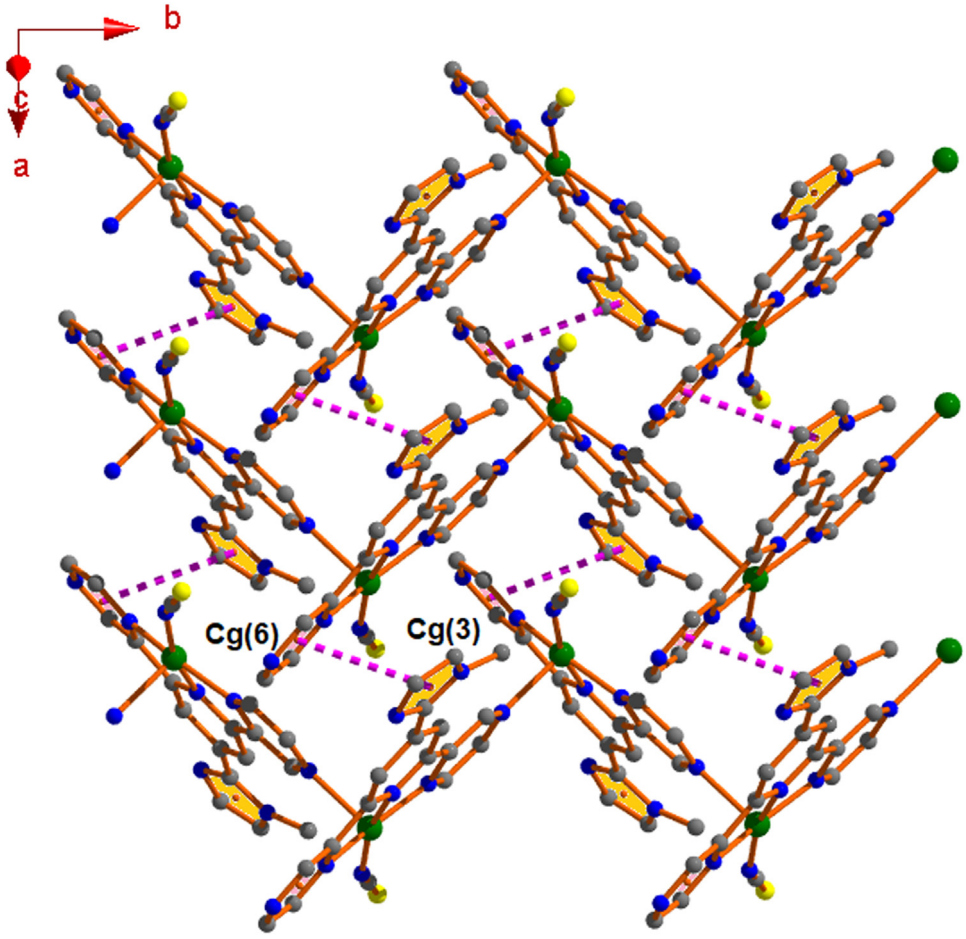

Fig. 10. Formation of a 2-D assembly through $\pi\cdots\pi$ interactions in complex **2** (aromatic hydrogen atoms have been omitted for clarity).

of the second **NL** ligand. Here, two five-membered chelate rings [(Cu1/N3/C7/C17/N6) and (Cu1/N3/C8/C10/N5)] are formed with bite angles [N3–Cu1–N6 = 80.11(9)° and N3–Cu1–N5 = 79.08(8)°] respectively. The average distance of Cu–N bonds in the equatorial plane is 1.996 Å [Cu1–N6 = 2.050(2) Å, Cu1–N3 = 1.932(2) Å, Cu1–N5 = 2.066(2) Å and Cu1–N8 = 1.937(3) Å]. The Cu(II) ion is deviated by a distance of 0.204 Å towards the apical nitrogen atom ($N4^b$, $b = 1 - x, 1/2 + y, 3/2 - z$) from the equatorial plane (N3, N5, N6 and N8). The axial Cu–N bond is comparatively larger [$Cu1–N4^b$ = 2.277(2) Å] than the other equatorial Cu–N bonds likely due to the more 'p' character of the orbital involved in the axial bond. The electrical charge on the metal center is taken care

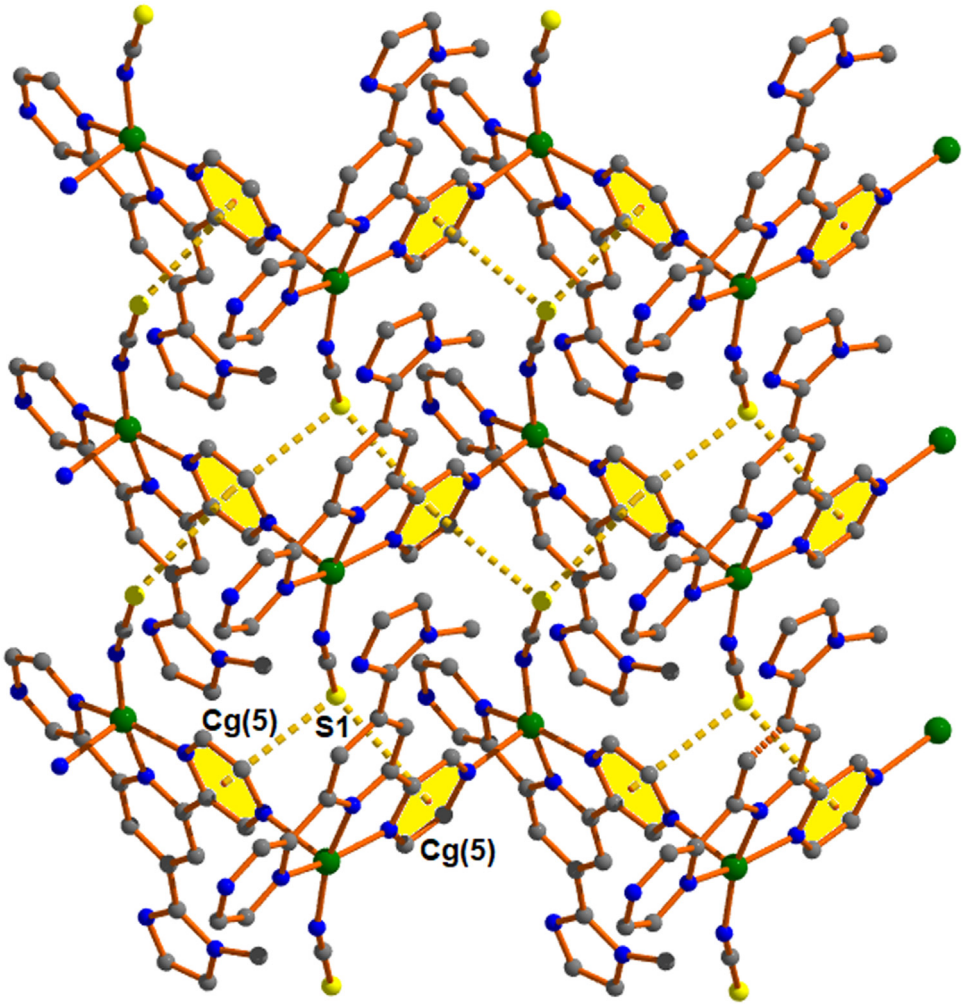

Fig. 11. Perspective view of 2-D architecture through sulphur(lone pair)···π interactions in complex **2** (aromatic hydrogen atoms have been omitted for clarity).

by one coordinated thiocyanate ion and one non-coordinated perchlorate ion.

In the solid state, the complex **2** is stabilized through C–H···O hydrogen bonds in addition with $\pi\cdots\pi$ stacking, $\pi\cdots\pi$ (chelate ring), anion···π and lone pair···π interactions (Tables S5-S7). The parallel 1-D zigzag chains are interlinked through face to face $\pi\cdots\pi$ interaction to build a 2-D layered structure (Fig. 9) in the *bc*-plane. The $\pi\cdots\pi$ interaction was executed between Cg(3) of one complex unit and Cg(3) of the other unit with the shortest centroid–centroid distance of 3.3969(19)Å (Table S5).

Fig. 10 shows that the 1-D parallel chains are interlinked through the self-complementary $\pi\cdots\pi$ stacking interactions between Cg(3) of one complex unit and Cg(6) of the other unit to form another two-dimensional (2-D) assembly in the *ab*-plane having an inter-planar spacing of 3.6803(18) Å (Table S6).

Again, the 2-D assembly is further stabilized by the lone pair···π interactions (shown in Fig. 11). The sulfur atom (S1) approaches (bifurcated) towards π-faces of two different Cg(5) units at $(-1 + x, y, z)$ and (-x, 1/2 + *y*, 3/2-z) with angles of 110.53(11)° and 95.28(10)° respectively (Table S7). For having a good sulphur(lone pair)···π interaction, the S···π distance should be less than the sum of their van der Waals radii (3.70 Å). Here, the average distance between sulfur atom (S1) and Cg(5) centroid is 3.543 Å; thus suggesting a significant lone pair···π interaction. Though the sulphur(lone pair)···π interaction is comparatively less frequent but it has been well appreciated in biological and model systems [113–116].

In the Fig. 12, the complex units of **2** (extracted from the polymeric chain) ensure to propagate a 1-D polymeric chain through $\pi\cdots\pi$(chelate ring) interaction (shown by orange dotted lines) between Cg(3) of one unit and Cg(1) (chelate ring) of the adjacent unit separated at a distance of 3.4980(16) Å (Table S6). The parallel chains are interconnected through C11–H11···O3 (119°) hydrogen bond (shown in aqua dotted line) and anion···π interaction (shown in pink dotted line). The said anion···π interaction involves one oxygen atom (O1) of the ClO_4^- anion and Cg(6) of the adjacent complex unit at (1-x, $-1/2 + y$, 3/2-z) with a shortest separation distance of 3.022(3) Å. Therefore, the influence of the unconventional $\pi\cdots\pi$(chelate ring) interactions along with anion···π and C–H···O hydrogen bonding interactions is responsible in building the extended 2-D architecture in the *ab*-plane (Fig. 12).

3.4. Theoretical study

PBE0-D3/def2-TZVP calculations have been used to study the chelate ring (CR) interactions described above that are relevant for the crystal packing of compound **1**. Compound **2** is a polymer and its solid-state architecture is basically governed by coordination bonds. In this case the theoretical study is limited to the characterization of the interactions described above in Fig. 12 using the NCI plot index analysis.

The molecular electrostatic potential (MEP) surface of compound **1** (including the counter ion and water molecule) has been firstly computed to analyze the most nucleophilic and electrophilic

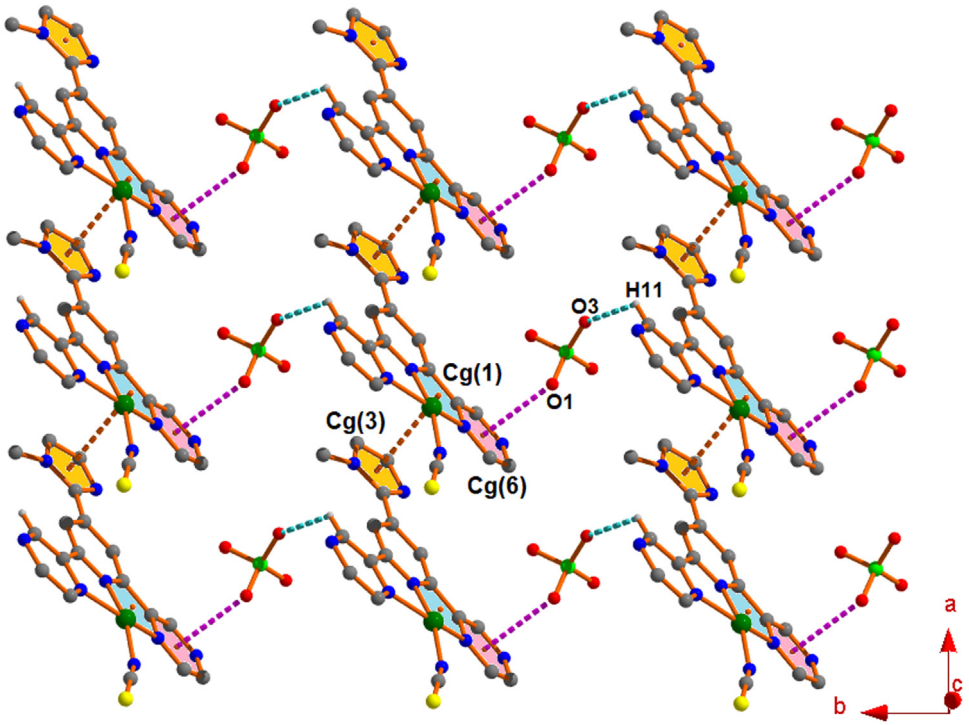

Fig. 12. Perspective view of 2-D architecture incorporating $\pi\cdots\pi$, anion$\cdots\pi$ and C–H···O hydrogen bonding interactions in complex **2** (other aromatic hydrogen atoms have been omitted for clarity).

parts of the molecules. As expected, the most negative MEP values are located at the perchlorate anion (–74 kcal/mol). The MEP values at the N-atoms of the azido ligand are also negative (–15 kcal/mol). The maximum MEP value (+75 kcal/mol) is located in a cleft that is under the influence of two aromatic H-atoms and one aliphatic H-atom (methyl group of the imidazole ring). The MEP values over the aromatic rings of the ligand are also large and positive, ranging from +21 to +47 kcal/mol. The MEP value over the chelate ring that is more distant from the perchlorate anion is also large and positive (+43 kcal/mol), thus adequate for interacting with electron rich atoms (as shown in Fig. 13).

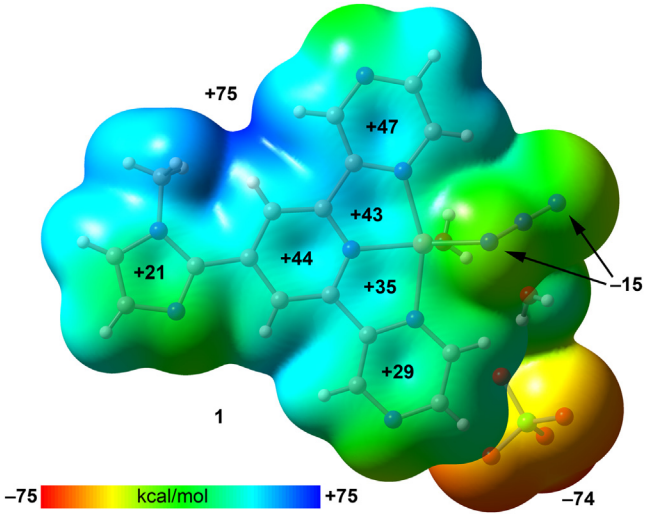

Fig. 13. MEP surface (isosurface 0.001 a.u.) of compound**1** at the PBE0-D3/def2-TZVP level of theory. The MEP values at selected points of the surfaces are given in kcal/mol.

The ion-pair nature of compound **1** anticipates a dominant role of electrostatic effects in its crystal packing. This is supported by the MEP surface analysis which shows the maximum and minimum MEP values located at the cationic and anionic moieties, respectively. In general, pure electrostatic forces are very strong and non-directional. Therefore, the final orientation of the cations and anions in the solid state is often influenced by other forces that are weaker but able to tune the final geometry of the assemblies found in their crystal structure.

As aforesaid in the structural description of **1** (Fig. 4), this compound forms interesting self-assembled dimers governed by the formation of two symmetrically equivalent lp$\cdots\pi$(CR) interactions. This DFT study is mainly focused on the investigation of this interaction. Fig. 14 shows the self-assembled dimer where, in addition to the lp$\cdots\pi$(CR) interactions, two anti-parallel displaced and conventional $\pi\cdots\pi$ interactions are formed. The dimerization energy is very large (–26.6 kcal/mol) due to the contribution of both types of π-stacking interactions. It should be mentioned that this interaction has been computed as a dimer where each monomeric fragment includes the water molecule and the perchlorate counter ion. Therefore, the H-bonds are not evaluated (considered as previously formed). In an effort to evaluate the contribution of the lp$\cdots\pi$(CR) interaction, we have used a reduced model where the ligand has been simplified (see Fig. 14b). Consequently, the energy is only reduced to –21.9 kcal/mol that is a rough estimation of the lp$\cdots\pi$(CR) interaction. Such large interaction energy agrees well with the MEP surface analysis shown in Fig. 13 that evidences a large and positive MEP value over the chelate ring and negative at the azido ligand. Therefore, it dominates the formation of this dimer. The contribution of the conventional $\pi\cdots\pi$ interactions can be estimated by difference, i.e. –4.7 kcal/mol, that is significantly weaker than the lp$\cdots\pi$(CR) interactions with the shortest centroid-to-centroid distances (see Fig. 14a).

The large dimerization energy obtained for the dimer of **1** is comparable to other interactions where anti-parallel π-stacking

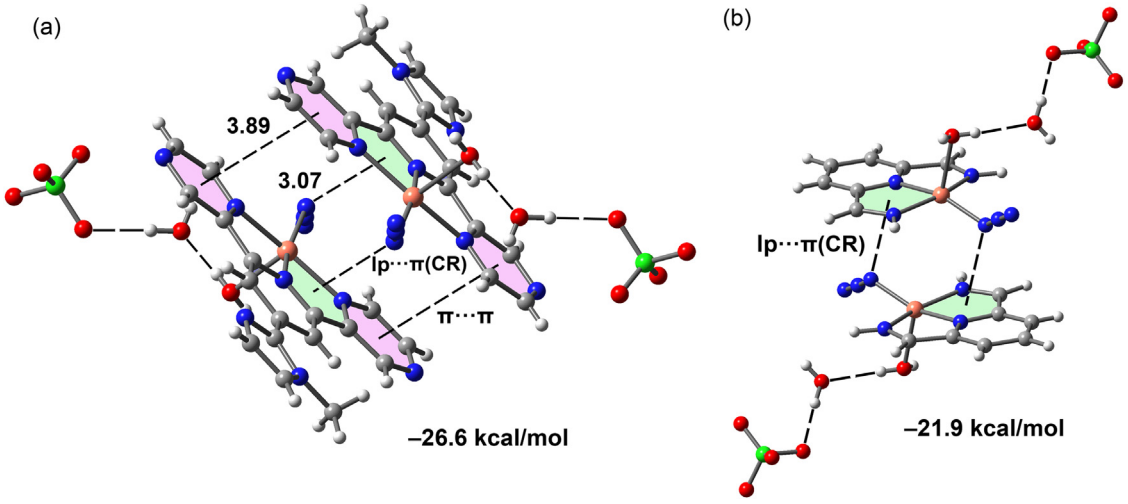

Fig. 14. (a) Dimer of compound **1**, π-stacking interactions shown as black dashed lines (distances in Å) (b) Reduced model of compound **1** used to estimate the lp···π(CR) interaction.

interactions in metal complexes with large and conjugated π-systems. It has been rationalized considering the large dipole moments of the metal complexes that are very polarized. For instances π-stacking interactions ranging from –25 to –35 kcal/mol have been reported for similar systems [117–125].

We have also computed the "Non-covalent Interaction plot" (NCI plot) index in order to characterize both types π-π stacking interactions in compound **1**. The NCI plot index is an intuitive visualization index that facilitates the visualization of non-covalent interactions and shows which molecular regions interact. The color scheme is a red-yellow-green-blue scale with red (repulsive) and blue (attractive). Yellow and green surfaces correspond to weak repulsive and weak attractive interactions, respectively. Fig. 15 shows the NCI plot index analysis of the self-assembled dimer of compound **1** using two different perspectives. The NCI plot reveals the

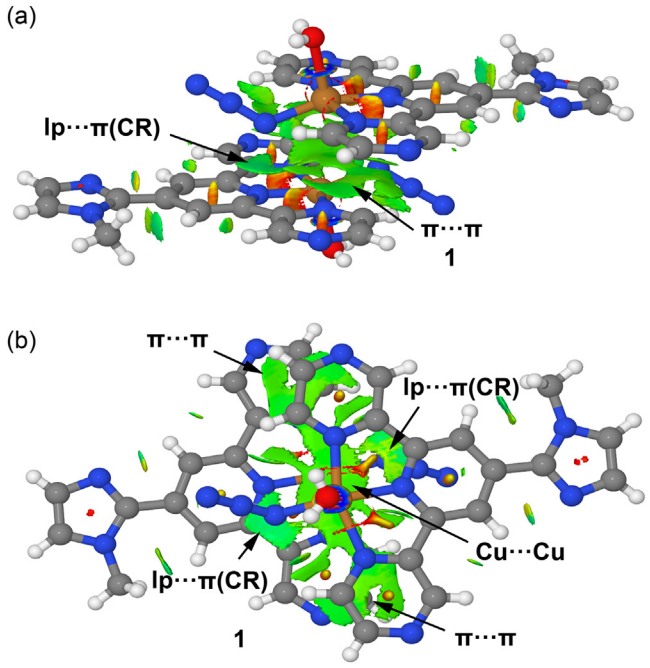

Fig. 15. NCI surface of the π-stacked assembly compound **1** using perspective (a) and on-top views (b) The gradient cut-off is ρ = 0.04 a.u., isosurface s = 0.35, and the color scale is −0.04 a.u.< ρ < 0.04 a.u.

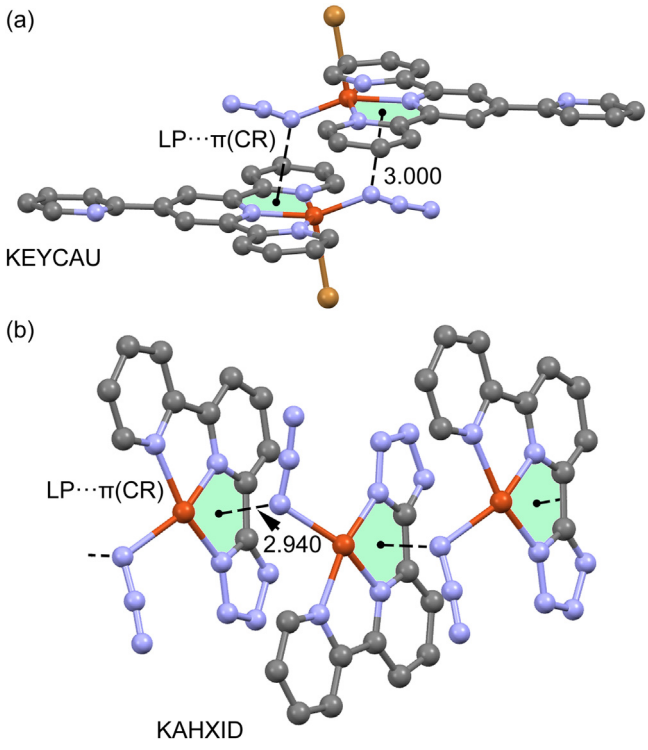

Fig. 16. Partial views of the solid state X-ray structures of refcodes KEYCAU (a) and KAHXID (b). Distances in Å. H-atoms omitted for clarity.

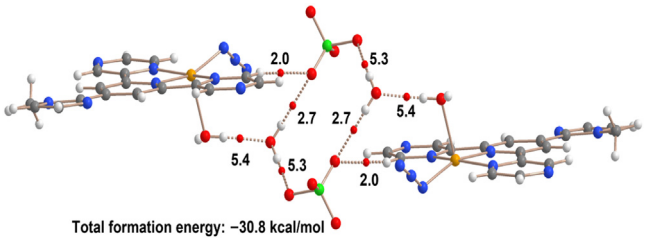

Fig. 17. QTAIM distribution of intermolecular bond critical points (small red spheres) and bond paths in the H-bonding assembly compound **1**. The dissociation energy of each H-bond is indicated adjacent to each bond critical point.

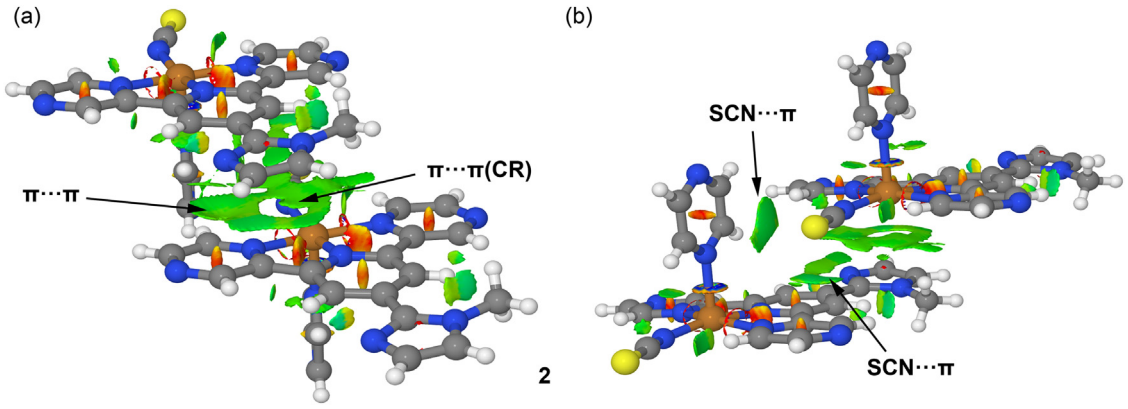

Fig. 18. NCI surface of the π-stacked assembly compound **2** using two different perspective views (a,b), (the gradient cut-off is ρ = 0.04 a.u., isosurface s = 0.35, and the color scale is −0.04a.u. < ρ < 0.04 a.u).

formation of green and extended isosurfaces upon dimerization that are located between the chelate rings and the N-atoms of the azido ligand, thus confirming the existence of the unconventional lp···π(CR) interaction. Moreover, the NCI plot also shows green isosurfaces located between the pyrazine aromatic rings, thus also confirming the existence of anti-parallel and displaced π···π stacking interactions. The NCIplot analysis also reveals a large and green isosurface between both Cu(II) ion, thus suggesting some type of metal···metal interaction that likely contributes to the large dimerization energy of the reduced model shown in Fig. 14b.

We have explored the Cambridge structural database (CSD) in order to investigate the prevalence of N_3···π(CR) interaction in Cu complexes with five membered (unsaturated) chelate rings. We have found only five structures in the CSD presenting similar LP···π(CR) interactions, which are summarized in Table 1. The LP···π(CR) interactions were not described by their original authors. The Cg···N distances are gathered in Table 1, which range from 2.938 to 3.016 Å, similar to the distance observed in compound **1** (3.070 Å). Two representative structures from this search are represented in Fig. 16. In KEYCAU structure, a self-assembled dimer is formed in the solid state that is very similar to that found in compound **1** (see Fig. 4) where two symmetrically equivalent LP···π(CR) interactions are formed. The other structure forms infinite 1D supramolecular assemblies in the solid state where the complex propagates in one direction due to the formation of the LP···π(CR) interactions. It is interesting to highlight that in all structures the LP-donor N-atom is the one that is coordinated to the Cu-atom.

The H-bonding network (anion−water cluster) described above in Fig. 5 has been also analysed theoretically using the quantum theory of atoms in molecules (QTAIM). The distribution of bond critical points and bond paths is represented in Fig. 17 along with the individual H-bond formation energies derived from the potential energy density predictor (E_{dis} = ½*V_r) proposed by Espinosa et al. [131] Each H-bond is characterized by a bond critical point connecting the H to the O-atom. The stronger H-bond corresponds to the one established between the coordinated and uncoordinated water molecules (5.4 kcal/mol) likely to the enhanced acidity of the water protons due to the coordination to Cu(II) metal center. The uncoordinated water molecule also establishes two additional H-bonds as donor with the perchlorate anions, one is strong (5.3 kcal/mol) and the other is more modest (2.7 kcal/mol) in agreement with the experimental bond angles as well as separation distances (Table S5). Finally, the QTAIM analysis further discloses the existence of C–H···O interactions between one aromatic H-atom of the ligand and the perchlorate anion. The interaction energy of this H-bond is the weakest one (2.0 kcal/mol). The total formation energy of this assembly is very large (–30.8 kcal/mol), thus confirming the importance of these H-bonding network in the crystal packing of compound **1**, in addition to the antiparallel π-stacking interactions described in Fig. 14.

Since compound **2** is a coordination polymer, we have used a dimeric model extracted from the polymeric chain (see Fig. 18) where pyrazine rings act as apical ligands for the Cu-atoms. The NCIplot analysis of the dimer is represented in Fig. 18 that reveals that the SCN ligand establishes conventional lp–π interactions with the aromatic rings. Since there is not a NCIplot isosurface located between the chelate ring and the SCN ligand, this analysis suggests that the chelate ring is not involved in the binding mechanism. In contrast, it reveals the existence of π···π(CR) interactions involving the five membered imidazole ring and the chelate ring (see Fig 18b). It is characterized by a green and extended NCIplot index isosurface that embraces the chelate ring and part of the fused pyrazine ring.

Table 1
CSD reference codes of Cu-complexes exhibiting N_3···π(CR) interactions. The distance from the N-atom to the ring centroid (Cg) is also indicated.

Ref. code	d(Cg···N), Å	Reference
FIBGIH	2.964	[126]
KAHXID	2.940	[127]
KEYKAU	3.000	[128]
KUCFIZ	2.938	[129]
LEXPAH	3.016	[130]

4. Concluding remarks

In conclusion, we have successfully synthesized two Cu(II) complexes (complex **1** and **2**) using 4-(1-methylimidazole)-2,6-di(pyrazinyl)pyridineas the backbone ligand with two different auxiliary ligands, established their solid-state crystal structures by single crystal X-ray diffraction study and explored the noncovalent interactions associated with their crystal structures. The structural insights reveal that intermolecular hydrogen bonding (C–H···N, C–H···O, O–H···N, O–H···O), π···π, π···π(chelate ring), anion···π, lone pair···π and lone pair···π(chelate ring) interactions play a significant role in crystal packing of the complexes in the solid state. A DFT study has been used to evaluate the cooperative influence of unconventional lone pair···π(CR) and conventional π···π stacking interactions in the dimeric distribution of complex **1** quantitatively and demonstrating that the former is stronger. Besides, the large formation energy of the perchlorate-water cluster (–30.8 kcal/mol) confirms its decisive role in the self assembly of complex **1**. The

sulfur (lone pair)···π and π···π(CR) interactions play a lead role in the crystal packing of complex **2**. The NCI plot index also exhibits the involvement of chelate ring to stabilize the crystal structures of the complexes significantly. Therefore, the present study undoubtedly helps to gain knowledge in this rising area of supramolecular chemistry. Finally, the CSD search discloses the existence of LP(N_3)···π(CR) in a few structures. However, further investigation in this topic will be conducted to extend the analysis to other elements, LP donors and ring sizes.

Declaration of Competing Interest

There are no conflicts to declare.

CRediT authorship contribution statement

Samit P., Sudipta P., A.F. and S.M.: investigation and methodology. A.F.: in silico studies. Samit P., Sudipta P. and S.M.: data curation. A.F. and S.M.: conceptualization, supervision, validation. A.F.: project administration. Samit P., A.F. and S.M. writing – original draft, writing – review and editing.

Acknowledgments

Samit P. is thankful to Council of Scientific and Industrial Research (CSIR, File no. 09/096(0947)/2018-EMR-I), New Delhi, for providing Senior Research Fellowship. We are thankful to Dr. Monotosh Mondal, Assistant Professor of Haldia Government College, Purba Medinipur 721657, West Bengal, India for helpful discussions. A. F. thanks the MICIU/AEI from Spain for financial support (Project PID2020-115637GB-I00, FEDER funds).

Supplementary materials

CCDC 2096470 and 2096471 contain the supplementary crystallographic data for complex 1 and complex 2 respectively. These data can be obtained free of charge via http://www.ccdc.cam.ac.uk/conts/retrieving.html, or from the Cambridge Crystallographic Data center, 12 Union Road, Cambridge CB2 1EZ, UK; fax: (+44) 1223-336-033; or e-mail: deposit@ccdc.cam.ac.uk.

Supplementary material associated with this article can be found, in the online version, at doi:10.1016/j.molstruc.2022.133358.

References

[1] A. Ciesielski, C.A. Palma, M. Bonini, P. Samorì, Towards supramolecular engineering of functional nanomaterials: pre-programming multi-component 2d self-assembly at solid-liquid interfaces, Adv. Mater. 22 (2010) 3506–3520 https://doi.org/, doi:10.1002/adma.201001582.
[2] D. Trauner, The chemist and the architect, Angew. Chem., Int. Ed. 57 (2017) 4177–4191, doi:10.1002/anie.201708325.
[3] K. Geng, T. He, R. Liu, S. Dalapati, K.T. Tan, Z. Li, S. Tao, Y. Gong, Q. Jiang, D. Jiang, Covalent organic frameworks: design, synthesis, and functions, Chem. Rev. 120 (2020) 8814–8933, doi:10.1021/acs.chemrev.9b00550.
[4] G.R. Desiraju, J.J. Vittal, A. Ramanan, Crystal Engineering: A Textbook, World Scientific Pub. Co. Inc., Singapore, 2011.
[5] G.R. Desiraju, Crystal engineering: from molecule to crystal, J. Am. Chem. Soc. 135 (2013) 9952–9967, doi:10.1021/ja403264c.
[6] M. Mirzaei, H. Eshtiagh-Hosseini, Z. Karrabi, K. Molčanov, E. Eydizadeh, J.T. Mague, A. Bauzá, A. Frontera, Crystal engineering with coordination compounds of Ni^{II}, Co^{II}, and Cr^{III} bearing dipicolinic acid driven by the nature of the noncovalent interactions, CrystEngComm 16 (2014) 5352–5363, doi:10.1039/C4CE00325J.
[7] J.J. Novoa, Intermolecular Interactions. Crystals: Fundamentals of Crystal Engineering, The Royal Society of Chemistry, London, 2018.
[8] M.D. Allendorf, V. Stavila, Crystal engineering, structure–function relationships, and the future of metal–organic frameworks, CrystEngComm 17 (2015) 229–246, doi:10.1039/C4CE01693A.
[9] A.K. Nangia, G.R. Desiraju, Crystal engineering: an outlook for the future, Angew. Chem., Int. Ed. 58 (2019) 4100–4107, doi:10.1002/anie.201811313.
[10] I. Gospodinov, K.V. Domasevitch, C.C. Unger, T.M. Klapötke, J. Stierstorfer, Midway between energetic molecular crystals and high-density energetic salts: crystal engineering with hydrogen bonded chains of polynitro bipyrazoles, Cryst. Growth Des. 20 (2020) 755–764, doi:10.1021/acs.cgd.9b01177.
[11] N.R. Mote, S.H. Chikkali, Hydrogen-bonding-assisted supramolecular metal catalysis, Chem.–Asian J. 13 (2018) 3623–3646, doi:10.1002/asia.201801302.
[12] R. Bu, Y. Xiong, X. Wei, H. Li, C. Zhang, Hydrogen bonding in CHON-containing energetic crystals: a review, Cryst. Growth Des. 19 (2019) 5981–5997, doi:10.1021/acs.cgd.9b00853.
[13] M. Madni, M.N. Ahmed, M. Hafeez, M. Ashfaq, M.N. Tahir, D.M. Gil, B. Galmés, S. Hameed, A. Frontera, Recurrent π–π stacking motifs in three new 4,5-dihydropyrazolyl–thiazole–coumarin hybrids: X-ray characterization, Hirshfeld surface analysis and DFT calculations, New J. Chem. 44 (2020) 14592–14603, doi:10.1039/D0NJ02931A.
[14] S. Pramanik, S. Pathak, S. Jana, M. Mondol, A. Frontera, S. Mukhopadhyay, An experimental and theoretical exploration of supramolecular interactions and photoresponse properties of two Ni(II) complexes, New J. Chem. 45 (2021) 12108–12119, doi:10.1039/D1NJ01363G.
[15] P. Manna, S.K. Seth, A. Das, J. Hemming, R. Prendergast, M. Helliwell, S.R. Choudhury, A. Frontera, S. Mukhopadhyay, Anion induced formation of supramolecular associations involving lone pair–π and anion–π interactions in Co(II) malonate complexes: experimental observations, Hirshfeld surface analyses and DFT studies, Inorg. Chem. 51 (2012) 3557–3571, doi:10.1021/ic202317f.
[16] L.A. Barrios, G. Aromi, A. Frontera, D. Quinonero, P.M. Deya, P. Gamez, O. Roubeau, E.J. Shotton, S.J. Teat, Coordination complexes exhibiting anion···π interactions: synthesis, structure, and theoretical studies, Inorg. Chem. 47 (2008) 5873–5881, doi:10.1021/ic800215r.
[17] C. Garau, D. Quiñonero, A. Frontera, P. Ballester, A. Costa, P.M. Deyà, Dual binding mode of *s*-triazine to anions and cations, Org. Lett. 5 (2003) 2227–2229, doi:10.1021/ol034650u.
[18] A. Rather, S.A. Wagay, R. Ali, Emergence of anion-π interactions: the land of opportunity in supramolecular chemistry and beyond, Coord. Chem. Rev. 415 (2020) 213327–213387, doi:10.1016/j.ccr.2020.213327.
[19] P. Pal, A. Hossain, R.M. Gomila, A. Frontera, S. Mukhopadhyay, Synthesis and crystal structure of the simultaneous binding of Ni(II) cation and chloride by the protonated 2,4,6 tris-(2-pyridyl)-1,3,5 triazine ligand: theoretical investigations of anion···π, π···π and hydrogen bonding interactions, New J. Chem. 45 (2021) 11689–11696, doi:10.1039/D1NJ01880A.
[20] C. Jia, H. Miao, B.P. Hay, Crystal structure evidence for the directionality of lone pair–π interactions: fact or fiction? Cryst. Growth Des. 19 (2019) 6806–6821, doi:10.1021/acs.cgd.9b01081.
[21] M. Savastano, C. García-Gallarín, M.D. López de la Torre, C. Bazzicalupi, A. Bianchi, M. Melguizo, Anion-π and lone pair-π interactions with *s*-tetrazine-based ligands, Coord. Chem. Rev. 397 (2019) 112–137, doi:10.1016/j.ccr.2019.06.016.
[22] J. Kozelka, Lone pair–π interactions in biological systems: occurrence, function, and physical origin, Eur. Biophys. J. 46 (2017) 729–737, doi:10.1007/s00249-017-1210-1.
[23] M. Chawla, E. Chermak, Q. Zhang, J.M. Bujnicki, R. Oliva L. Cavallo, Occurrence and stability of lone pair–π stacking interactions between ribose and nucleobases in functional RNAs, Nucleic Acids Res 45 (2017) 11019–11032, doi:10.1093/nar/gkx757.
[24] K. Kalra, S. Gorle, L. Cavallo, R. Oliva, M. Chawla, Occurrence and stability of lone pair-π and OH–π interactions between water and nucleobases in functional RNAs, Nucleic Acids Res 48 (2020) 5825–5838, doi:10.1093/nar/gkaa345.
[25] S. Maity, T.K. Ghosh, R.M. Gomila, A. Frontera, A. Ghosh, Recurrent π(arene)···π(chelate ring) motifs in four trinuclear $Cu^{II}_2M^{II}$ (M = Cd/Zn) complexes derived from an unsymmetrical N_2O_2 donor ligand: structural and theoretical investigations, CrystEngComm 22 (2020) 7673–7683, doi:10.1039/D0CE01219J.
[26] S. Mirdya, S. Roy, S. Chatterjee, A. Bauza, A. Frontera, S. Chattopadhyay, Importance of π-interactions involving chelate rings in addition to the tetrel bonds in crystal engineering: a combined experimental and theoretical study on a series of hemi- and holodirected nickel(II)/lead(II) complexes, Cryst. Growth Des. 19 (2019) 5869–5881, doi:10.1021/acs.cgd.9b00881.
[27] D.P. Malenov, G.V. Janjić, V.B. Medaković, M.B. Hall, S.D. Zarić, Noncovalent bonding: Stacking interactions of chelate rings of transition metal complexes, *Coord.* Chem. Rev. 345 (2017) 318–341, doi:10.1016/j.ccr.2016.12.020.
[28] D.P. Malenov, D.Ž. Veljković, M.B. Hall, E.N. Brothers, S.D. Zarić, Influence of chelate ring type on chelate–chelate and chelate–aryl stacking: the case of nickel bis(dithiolene), Phys. Chem. Chem. Phys. 21 (2019) 1198–1206, doi:10.1039/C8CP06312E.
[29] D.P. Malenov, S.D. Zarić, Strong stacking interactions of metal–chelate rings are caused by substantial electrostatic component, Dalton Trans 48 (2019) 6328–6332, doi:10.1039/C9DT00182D.
[30] S.L. Tan, S.M. Lee, K.M. Lo, A. Otero-de-la-Roza, E.R.T. Tiekink, Experimental and computational evidence for a stabilising C–Cl(lone-pair)···π(chelate-ring) interaction, CrystEngComm 23 (2021) 119–130, doi:10.1039/D0CE01478H.
[31] T. Maity, H. Mandal, A. Bauza, B.C. Samanta, A. Frontera, S.K. Seth, Quantifying conventional C–H···π(aryl) and unconventional C–H···π(chelate) interactions in dinuclear Cu(II) complexes: experimental observations, Hirshfeld surface and theoretical DFT study, New J. Chem. 42 (2018) 10202–10213, doi:10.1039/C8NJ00747K.
[32] E.R.T. Tiekink, The remarkable propensity for the formation of C–H···π(chelate ring) interactions in the crystals of the first-row transition metal dithiocarbamates and the supramolecular architectures they sustain, CrystEngComm 22 (2020) 7308–7333, doi:10.1039/D0CE00289E.
[33] B. Dutta, S.M. Pratik, S. Jana, C. Sinha, A. Datta, M.H. Mir, Novel

Br···π(chelate) interaction in a 1D coordination polymer revealing aromaticity, ChemistrySelect 3 (2018) 4289–4291, doi:10.1002/slct.201800738.
[34] E.R.T. Tiekink, Supramolecular architectures sustained by delocalised C–I···π(arene) interactions in molecular crystals and the propensity of their formation, CrystEngComm 23 (2021) 904–928, doi:10.1039/D0CE01677B.
[35] H. Masui, Metalloaromaticity, Coord. Chem. Rev. 219–221 (2001) 957–992, doi:10.1016/S0010-8545(01)00389-7.
[36] A. Castiñeiras, A.G. Sicilia-Zafra, J.M. Gonzáles-Pérez, D. Choquesillo-Lazarte J. Niclós-Gutiérrez, Intramolecular "aryl–metal chelate ring" π,π-interactions as structural evidence for metalloaromaticity in (aromatic α,α'-diimine)–copper(II) chelates: molecular and crystal structure of aqua(1,10-phenanthroline)(2-benzylmalonato)copper(II) three-hydrate, Inorg. Chem. 41 (2002) 6956–6959, doi:10.1021/ic026004h.
[37] L. Wang, B. Song, S. Khalife, Y. Li, L.-J. Ming, S. Bai, Y. Xu, H. Yu, M. Wang, H. Wang, X. Li, Introducing seven transition metal ions into terpyridine-based supramolecules: self-assembly and dynamic ligand exchange study, J. Am. Chem. Soc. 142 (2020) 1811–1821, doi:10.1021/jacs.9b09497.
[38] G. Baronea, G. Gennaroa, A.M. Giuliania, M. Giustini, Interaction of Cd(II) and Ni(II) terpyridine complexes with model polynucleotides: a multidisciplinary approach, RSC Adv 6 (2016) 4936–4945, doi:10.1039/C5RA24919H.
[39] A. Wild, A. Winter, F. Schlütter, U.S. Schubert, Advances in the field of π-conjugated 2,2′:6′,2″-terpyridines, Chem. Soc. Rev. 40 (2011) 1459–1511, doi:10.1039/C0CS00074D.
[40] D. Saccone, C. Magistris, N. Barbero, P. Quagliotto, C. Barolo, G. Viscardi, Terpyridine and quaterpyridine complexes as sensitizers for photovoltaic applications, Materials 9 (2016) 137–174, doi:10.3390/ma9030137.
[41] P. Liu, G. Shi, X. Chen, Terpyridine-containing π-conjugated polymers for light-emitting and photovoltaic materials, Front. Chem. 8 (2020) 923–929, doi:10.3389/fchem.2020.592055.
[42] M.M. Milutinović, S.K.C. Elmroth, G. Davidović, A. Rilak, O. Klisurić, I. Bratsos, Ž.D. Bugarčić, Kinetic and mechanistic study on the reactions of ruthenium(II) chlorophenyl terpyridine complexes with nucleobases, oligonucleotides and DNA, Dalton Trans. 46 (2017) 2360–2369, doi:10.1039/C6DT04254F.
[43] C. Li, F. Xu, Y. Zhao, W. Zheng, W. Zeng, Q. Luo, Z. Wang, K. Wu, J. Du, F. Wang, Platinum(II) terpyridine anticancer complexes possessing multiple mode of DNA interaction and EGFR inhibiting activity, Front. Chem. 8 (2020) 210–224, doi:10.3389/fchem.2020.00210.
[44] C. Bai, F.H. Wei, H.M. Hu, L. Yan, X. Wang, G.L. Xue, New highly luminescent europium(III) complex covalently bonded with titania-based host via using a terpyridine carboxylate derivative linker for fluorescence sensing, J. Lumin. 227 (2020) 117545–117555, doi:10.1016/j.jlumin.2020.117545.
[45] P. Pal, T. Ganguly, S. Das, S. Baitalik, pH-Responsive colorimetric, emission and redox switches based on Ru(II)–terpyridine complexes, Dalton Trans 50 (2021) 186–196, doi:10.1039/D0DT03537H.
[46] Y. Wang, X.W. Gao, J. Li, D. Chao, Merging an organic TADF photosensitizer and a simple terpyridine–Fe(III) complex for photocatalytic CO_2 reduction, Chem. Commun. 56 (2020) 12170–12173, doi:10.1039/D0CC05047D.
[47] R. Fernández-Terán, L. Sévery, Living long and prosperous: productive intraligand charge-transfer states from a rhenium(I) terpyridine photosensitizer with enhanced light absorption, Inorg. Chem. 60 (2021) 1334–1343, doi:10.1021/acs.inorgchem.0c01939.
[48] C. Wei, Y. He, X. Shi, Z. Song, Terpyridine-metal complexes: applications in catalysis and supramolecular chemistry, Coord. Chem. Rev. 385 (2019) 1–19, doi:10.1016/j.ccr.2019.01.005.
[49] A. Winter, U.S. Schubert, Metal-terpyridine complexes in catalytic application–a spotlight on the last decade, ChemCatChem 12 (2020) 1–52, doi:10.1002/cctc.201902290.
[50] M. Elcheikh Mahmoud, H. Audi, A. Assoud, T.H. Ghaddar, M. Hmadeh, Metal–organic framework photocatalyst incorporating bis(4′-(4-carboxyphenyl)-terpyridine)ruthenium(II) for visible-light-driven carbon dioxide reduction, J. Am. Chem. Soc. 141 (2019) 7115–7121, doi:10.1021/jacs.9b01920.
[51] D. Luo, T. Zuo, J. Zheng, Z.-H. Long, X.-Z. Wang, Y.-L. Huang, X.-P. Zhou, D. Li, Enabling photocatalytic activity of [Ru(2,2′:6′,2″-terpyridine)$_2$]$^{2+}$ integrated into a metal–organic framework, Mater. Chem. Front. 5 (2021) 2777–2782, doi:10.1039/D1QM00024A.
[52] B.Z. Momeni, F. Rahimi, M. Torrei, F. Rominger, Hirshfeld surface analysis, luminescence and thermal properties of three first-row transition metal complexes containing 4′-hydroxy-2,2′:6′,2″-terpyridine: application for preparation of nano metal oxides, Appl. Organometal. Chem. 34 (2020) 5613–5635, doi:10.1002/aoc.5613.
[53] A.M. Maron, K. Choroba, J.G. Małecki, S. Kula, E. Malicka, Platinum(II) coordination compound with 4′-[4-(dimethylamino)phenyl]-2,2′:6′,2″-terpyridine–the new insight into the luminescence behavior and substituent effect, Polyhedron 182 (2020) 114502–114511, doi:10.1016/j.poly.2020.114502.
[54] B.Z. Momeni, S.K. Anari, M. Torrei, J. Janczak, Crystal exploring, Hirshfeld surface analysis, and properties of 4′-(furan-2-yl)-2,2′:6′,2″-terpyridine complexes of nickel (II): new precursors for the synthesis of nanoparticles, Appl. Organometal. Chem. 35 (2021) 6179–6201, doi:10.1002/aoc.6179.
[55] E.U. Mughal, M. Mirzaei, A. Sadiq, S. Fatima, A. Naseem, N. Naeem, N. Fatima, S. Kausar, A.A. Altaf, M.N. Zafar, B.A. Khan, Terpyridine-metal complexes: effects of different substituents on their physico-chemical properties and density functional theory studies, R. Soc. Open Sci. 7 (2020) 201208–201239, doi:10.1098/rsos.201208.
[56] S.M. Elahi, M. Raizada, P.K. Sahu, S. Konar, Terpyridine-based 3D metal–organic-frameworks: a structure–property correlation, Chem. Eur. J. 27 (2021) 5858–5870, doi:10.1002/chem.202004651.
[57] F.A. Mautner, J.H. Albering, E.V. Harrelson, A.A. Gallo, S.S. Massoud, N-bonding vs. S-bonding in thiocyanato-copper(II) complexes, J. Mol. Struct. 1006 (2011) 570–575, doi:10.1016/j.molstruc.2011.10.005.
[58] S.S. Massoud, M. Dubin, A.E. Guilbeau, M. Spell, R. Vicente, P. Wilfling, R.C. Fischer, F.A. Mautner, Azido- and thiocyanato-cobalt(II) complexes based pyrazole ligands, Polyhedron 78 (2014) 135–140, doi:10.1016/j.poly.2014.04.025.
[59] F.A. Mautner, M. Traber, P. Jantscher, R.C. Fischer, K. Reichmann, R. Vicente, N. Arafat, S.S. Massoud, Thiocyanato-metal(II) and azido-cobalt(III) complexes with hydroxymethylpyridines, Polyhedron 161 (2019) 309–316, doi:10.1016/j.poly.2019.01.030.
[60] A. Di Santo, H. Perez, G.A. Echeverria, O.E. Piro, R.A. Iglesias, R.E. Carbonio, A. Ben Altabef, D.M. Gil, Exploring weak intermolecular interactions in thiocyanate-bonded Zn(II) and Cd(II) complexes with methylimidazole: crystal structures, Hirshfeld surface analysis and luminescence properties, RSC Adv 8 (2018) 23891–23902, doi:10.1039/C8RA04452J.
[61] M. Mondal, S. Jana, M.G.B. Drew, A. Ghosh, Application of two Cu(II)-azido based 1D coordination polymers in optoelectronic device: structural characterization and experimental studies, Polymer 204 (2020) 122815–122824, doi:10.1016/j.polymer.2020.122815.
[62] P. Ghorai, P. Brandão, S. Benmansour, C.J.G. García, A. Saha, Azido and thiocyanato bridged dinuclear Ni(II) complexes involving 8-aminoquinoline based Schiff base as blocking ligands: Crystal structures, ferromagnetic properties and magneto-structural correlations, Polyhedron 188 (2020) 114708–114715, doi:10.1016/j.poly.2020.114708.
[63] C.D. Mekuimemba, F. Conan, A.J. Mota, M.A. Palacios, E. Colacio, S. Triki, On the magnetic coupling and spin crossover behavior in complexes containing the head-to-tail [Fe$^{II}_2$(μ-SCN)$_2$] bridging unit: a magnetostructural experimental and theoretical study, Inorg. Chem. 57 (2018) 2184–2192, doi:10.1021/acs.inorgchem.7b03082.
[64] K. Vrieze, G. Van Koten, Comprehensive Coordination Chemistry, 2, Pergamon Oxford, 1987, p. 225.
[65] E.I. Solomon, D.E. Heppner, E.M. Johnston, J.W. Ginsbach, J. Cirera, M. Qayyum, M.T. Kieber-Emmons, C.H. Kjaergaard, R.G. Hadt, L. Tian, Copper active sites in biology, Chem. Rev. 114 (2014) 3659–3853, doi:10.1021/cr400327t.
[66] K. Choroba, B. Machura, S. Kula, L.R. Raposo, A.R. Fernandes, R. Kruszynski, K. Erfurt, L.S. Shul, Y.N. Kozlov, G.B. Shul, Copper(II) complexes with 2,2′:6′,2″-terpyridine, 2,6-di(thiazol-2-yl)pyridine and 2,6-di(pyrazin-2-yl)pyridine substituted with quinolines. Synthesis, structure, antiproliferative activity, and catalytic activity in the oxidation of alkanes and alcohols with peroxides, Dalton Trans. 48 (2019) 12656–12673, doi:10.1039/C9DT01922G.
[67] R. Nasani, M. Saha, S.M. Mobin, L.M.D.R.S. Martins, A.J.L. Pombeiro, A.M. Kirillov, S. Mukhopadhyay, Copper–organic frameworks assembled from *in situ* generated 5-(4-pyridyl)tetrazole building blocks: synthesis, structural features, topological analysis and catalytic oxidation of alcohols, Dalton Trans. 43 (2014) 9944, doi:10.1039/C4DT00531G.
[68] Z. Ma, L. Wei, E.C.B.A. Alegria, L.M.D.R.S. Martins, M.F.C.G. da Silva, A.J.L. Pombeiro, Synthesis and characterization of copper(II) 4′-phenyl-terpyridine compounds and catalytic application for aerobic oxidation of benzylic alcohols, Dalton Trans. 43 (2014) 4048–4058, doi:10.1039/C3DT53054J.
[69] J.Z. Gu, M. Wen, Y. Cai, Z.F. Shi, A.S. Arol, M.V. Kirillova, A.M. Kirillov, Metal–organic architectures assembled from multifunctional polycarboxylates: hydrothermal self-assembly, structures, and catalytic activity in alkane oxidation, Inorg. Chem. 58 (2019) 2403, doi:10.1021/acs.inorgchem.8b02926.
[70] K. Choroba, B. Machura, A. Szlapa-Kula, J.G. Malecki, L. Raposo, C. Roma Rodrigues, S. Cordeiro, P.V. Baptista, A.R. Fernandes, Square planar Au(III), Pt(II) and Cu(II) complexes with quinoline-substituted 2,2′:6′,2″-terpyridine ligands: from *in vitro* to *in vivo* biological properties, Eur. J. Med. Chem. 218 (2021) 113404–113423, doi:10.1016/j.ejmech.2021.113404.
[71] Y. Liu, S.C. Yiu, C.L. Ho, W.Y. Wong, Recent advances in copper complexes for electrical/light energy conversion, Coord. Chem. Rev. 375 (2018) 514–557, doi:10.1016/j.ccr.2018.05.010.
[72] C. Icsel, V.T. Yilmaz, S. Aydinlik, M. Aygun, New manganese(II), iron(II), cobalt(II), nickel(II) and copper(II) saccharinate complexes of 2,6-bis(2-benzimidazolyl)pyridine as potential anticancer agents, Eur. J. Med. Chem. 202 (2020) 112535–112545, doi:10.1016/j.ejmech.2020.112535.
[73] C. Wu, J. Wang, J. Shen, C. Zhang, Z. Wu, H. Zhou, A colorimetric quinoline-based chemosensor for sequential detection of copper ion and cyanide anions, Tetrahedron 73 (2017) 5715–5719, doi:10.1016/j.tet.2017.08.010.
[74] H.Q. Li, X.Q. Sun, T. Zheng, Z.X. Xu, Y.X. Song, X.H. Gu, Coumarin-based multifunctional chemosensor for arginine/lysine and Cu^{2+}/Al^{3+} ions and its Cu^{2+} complex as colorimetric and fluorescent sensor for biothiols, Sens. Actuators, B 279 (2019) 400–409, doi:10.1016/j.snb.2018.10.017.
[75] A. Hussain, M.F. AlAjmi, T. Rehman, S. Amir, F.M. Husain, A. Alsalme, M.A. Siddiqui, A.A. AlKhedhairy, R.A. Khan, Copper(II) complexes as potential anticancer and nonsteroidal anti-inflammatory agents: in vitro and in vivo studies, Sci. Rep. 9 (2019) 5237–5254, doi:10.1038/s41598-019-41063-x.
[76] J. Karges, K. Xiong, O. Blacque, H. Chao, G. Gasser, Highly cytotoxic copper(II) terpyridine complexes as anticancer drug candidates, Inorganica Chimica Acta 516 (2021) 120137–120143, doi:10.1016/j.ica.2020.120137.
[77] F. Cheng, N. Tang, K. Miao, F. Wang, A Dinuclear Ruthenium(II) Polypyridyl Complex Containing A terpy-like Fragment for Cu^{2+} Probing, Z. Anorg. Allg. Chem. 640 (2014) 1816–1821, doi:10.1002/zaac.201300662.
[78] Y.Q. Pan, X. Xu, Y. Zhang, Y. Zhang, W.K. Dong, A highly sensitive and selective bis(salamo)-type fluorescent chemosensor for identification of Cu^{2+} and the

continuous recognition of S^{2-}, Arginine and Lysine, Spectrochim. Acta, Part A 229 (2020) 117927–117937, doi:10.1016/j.saa.2019.117927.
[79] Z.-Y. Li, J.-S. Yang, R.-B. Liu, J.-J. Zhang, S.-Q. Liu, J. Nia, C.-Y. Duan, Two one-dimensional compounds based on pyramidal {$TbCu_4$} units and formate ligand: chair-like $[(H_2O)_2(ClO_4)_2]^{2-}$ clusters and slow relaxation of magnetization, Dalton Trans. 41 (2012) 13264–13267, doi:10.1039/C2DT32147E.
[80] S.S. Bhat, V.K. Revankar, N. Shivalingegowda, N.K. Lokanath, A fluorophore-labelled copper complex: Crystal structure, hybrid cyclic water-perchlorate cluster and biological properties, Acta Crystallogr. C 73 (9) (2017) 710–717, doi:10.1107/S2053229617011639.
[81] T. Mandal, A. Dey, S. Pathak, M.M. Islam, S. Konar, J. Ortega-Castro, S.K. Seth, P.P. Ray, A. Frontera, S. Mukhopadhyay, Structures, photoresponse properties and DNA binding abilities of 4-(4-pyridinyl)-2-pyridone salts, RSC Adv 9 (2019) 9663–9677, doi:10.1039/C9RA00666D.
[82] Bruker, SMART ν5.631, Bruker AXS Inc., Madison, WI, USA, 2001.
[83] G.M. Sheldrick, SHELXT-2014, University of Göttingen, 2014.
[84] G.M. Sheldrick, Crystal structure refinement with *SHELXL*, Acta Crystallogr., Sect. C: Struct. Chem. 71 (2015) 3–8, doi:10.1107/S2053229614024218.
[85] M.J. Frisch, G.W. Trucks, H.B. Schlegel, G.E. Scuseria, M.A. Robb, J.R. Cheeseman, G. Scalmani, V. Barone, B. Mennucci, G.A. Petersson, H. Nakatsuj, M. Caricato, X. Li, H.P. Hratchian, A.F. Iamaylov, J. Bloino, G. Zheng, J.L. Sonnenberg, M. Hada, M. Ehara, K. Toyota, R. Fukuda, J. Hasegawa, M. Ishida, T. Nakajima, Y. Honda, O. Kitao, H. Nakai, T. Vreven, J.A. Montgomery Jr, J.E. Peralta, F. Ogliaro, M. Bearpark, J.J. Heyd, E. Brothers, K.N. Kudin, V.N. Staroverov, R. Kobayashi, J. Normand, K. Raghavachari, A. Rendell, J.C. Burant, S.S. Lyengar, J. Tomasi, M. Cossi, N. Rega, J.M. Millam, M. Klene, J.E. Knox, J.B. Cross, V. Bakken, C. Adamo, J. Jaramillo, R. Gomperts, R.E. Stratmann, O. Yazyev, A.J. Austin, R. Cammi, C. Pomelli, J.W. Ochterski, R.L. Martin, K. Morokuma, V.G. Zakrzewski, G.A. Voth, P. Salvador, J.J. Dannenberg, S. Dapprich, A.D. Daniels, O. Farkas, J.B. Foresman, J.V. Ortiz, J. Cioslowski, D.J. Fox, Gaussian 09, Revision A.1, Gaussian Inc., Wallingford CT, 2016.
[86] S.F. Boys, F. Bernardi, The calculation of small molecular interactions by the differences of separate total energies. Some procedures with reduced errors, Mol. Phys. 19 (1970) 553–556, doi:10.1080/00268977000101561.
[87] S. Grimme, J. Antony, S. Ehrlich, H. Krieg, A consistent and accurate *ab initio* parametrization of density functional dispersion correction (DFT-D) for the 94 elements H-Pu, J. Chem. Phys. 132 (2010) 154104–154123, doi:10.1063/1.3382344.
[88] P. Manna, S.K. Seth, M. Mitra, S.R. Choudhury, A. Bauzá, A. Frontera, S. Mukhopadhyay, Experimental and computational study of counterintuitive $ClO_4^-\cdots ClO_4^-$ interactions and the interplay between π^+–π and anion$\cdots\pi^+$ interactions, Cryst. Growth Des. 14 (2014) 5812–5821, doi:10.1021/cg5014126.
[89] M. Mirzaei, H. Eshtiagh-Hosseini, Z. Bolouri, Z. Rahmati, A. Esmaeilzadeh, A. Hassanpoor, A. Bauza, P. Ballester, M. Barceló-Oliver, J.T. Mague, B. Notash, A. Frontera, Rationalization of noncovalent interactions within six new M^{II}/8-aminoquinoline supramolecular complexes (M^{II} = Mn, Cu, and Cd): a combined experimental and theoretical DFT study, Cryst. Growth Des. 15 (2015) 1351–1361, doi:10.1021/cg501752e.
[90] Y.V. Torubaev, I.V. Skabitsky, A.V. Rozhkov, B. Galmes, A. Frontera, V. Yu. Kukushkin, Highly polar stacking interactions wrap inorganics in organics: lone-pair–π-hole interactions between the PdO_4 core and electron-deficient arenes, Inorg. Chem. Front. 8 (2021) 4965–4975, doi:10.1039/D1QI01067K.
[91] V.V. Suslonov, N.S. Soldatova, D.M. Ivanov, B. Galmes, A. Frontera, G. Resnati, P.S. Postnikov, V. Yu. Kukushkin, N.A. Bokach, Diaryliodonium tetrachloroplatinates(II): recognition of a trifurcated metal-involving μ_3-I$\cdots$(Cl, Cl, Pt) halogen bond, Cryst. Growth Des. 21 (2021) 5360–5372, doi:10.1021/acs.cgd.1c00654.
[92] A.V. Rozhkov, I.V. Ananyev, A.A. Petrov, B. Galmes, A. Frontera, N.A. Bokach, V. Yu. Kukushkin, Ligand steric hindrances switch bridging (μ_2-I)$\cdots$O, O to two-center I$\cdots$O halogen-bonding mode in the assembly of diketonate copper(II) species, Cryst. Growth Des. 21 (2021) 4073–4082, doi:10.1021/acs.cgd.1c00373.
[93] S.V. Baykov, K.K. Geyl, D.M. Ivanov, R.M. Gomila, A. Frontera, V. Yu. Kukushkin, Azine steric hindrances switch halogen bonding to N-arylation upon interplay with σ-hole donating haloarenenitriles, Chem. Asian J. 16 (2021) 1445–1455, doi:10.1002/asia.202100282.
[94] L.E. Zelenkov, A.A. Eliseeva, S.V. Baykov, V.V. Suslonov, B. Galmes, A. Frontera, V. Yu. Kukushkin, D.M. Ivanov, N.A. Bokach, Electron belt-to-σ-hole switch of noncovalently bound iodine(I) atoms in dithiocarbamate metal complexes, Inorg. Chem. Front. 8 (2021) 2505–2517, doi:10.1039/D1QI00314C.
[95] Z.M. Efimenko, A.A. Eliseeva, D.M. Ivanov, B. Galmes, A. Frontera, N.A. Bokach, V. Yu. Kukushkin, Bifurcated μ_2-I$\cdots$(N,O) halogen bonding: the case of (nitrosoguanidinate) Ni^{II} cocrystals with iodine(I)-based σ-hole donors, Cryst. Growth Des. 21 (2021) 588–596, doi:10.1021/acs.cgd.0c01408.
[96] L.E. Zelenkov, D.M. Ivanov, E.K. Sadykov, A.Bokach N, B. Galmes, A. Frontera, V. Yu. Kukushkin, Semicoordination bond breaking and halogen bond making change the supramolecular architecture of metal-containing aggregates, Cryst. Growth Des. 20 (2020) 6956–6965, doi:10.1021/acs.cgd.0c00999.
[97] N.S. Soldatova, P.S. Postnikov, V.V. Suslonov, T. Yu. Kissler, D.M. Ivanov, M.S. Yusubov, B. Galmes, A. Frontera, V. Yu. Kukushkin, Diaryliodonium as a double σ-hole donor: the dichotomy of thiocyanate halogen bonding provides divergent solid state arylation by diaryliodonium cations, Org. Chem. Front. 7 (2020) 2230–2242, doi:10.1039/D0QO00678E.
[98] A.V. Rozhkov, A.A. Eliseeva, S.V. Baykov, B. Galmes, A. Frontera, V. Yu. Kukushkin, One-pot route to x-perfluoroarenes (X = Br, I) based on Fe^{III}-assisted C–F functionalization and utilization of these arenes as building blocks for crystal engineering involving halogen bonding, Cryst. Growth Des. 20 (2020) 5908–5921, doi:10.1021/acs.cgd.0c00606.
[99] A.V. Rozhkov, I.V. Ananyev, R.M. Gomila, A. Frontera, V. Yu Kukushkin, π-Hole$\cdots d_{z^2}[Pt^{II}]$ interactions with electron-deficient arenes enhance the phosphorescence of Pt^{II}-based luminophores, Inorg. Chem. 59 (2020) 9308–9314, doi:10.1021/acs.inorgchem.0c01170.
[100] E.A. Katlenok, M. Haukka, O.V. Levin, A. Frontera, V. Yu. Kukushkin, Supramolecular assembly of metal complexes by (aryl)I$\cdots$d $[Pt^{II}]$ halogen bonds, Chem. Eur. J. 26 (2020) 7692–7701, doi:10.1002/chem.202001196.
[101] J. Contreras-García, E.R. Johnson, S. Keinan, R. Chaudret, J.-P. Piquemal, D.N. Beratan, W. Yang, NCIPLOT: A program for plotting noncovalent interaction regions, J. Chem. Theory Comput. 7 (2011) 625–632, doi:10.1021/ct100641a.
[102] Ł. Jaremko, A.M. Kirillov, P. Smoleński, A.J.L. Pombeiro, Engineering coordination and supramolecular copper–organic networks by aqueous medium self-assembly with 1,3,5-triaza-7-phosphaadamantane (PTA), Cryst. Growth Des. 9 (2009) 3006–3010, doi:10.1021/cg900334w.
[103] K.R. Gruenwald, A.M. Kirillov, M. Haukka, J. Sanchiz, A.J.L. Pombeiro, Mono-, di- and polynuclear copper(II) compounds derived from N-butyldiethanolamine: structural features, magnetism and catalytic activity for the mild peroxidative oxidation of cyclohexane, Dalton Trans. (2009) 2109–2120, doi:10.1039/B813160K.
[104] P.J. Figiel, A.M. Kirillov, M.F.C. Guedes da Silva, J. Lasri, A.J.L. Pombeiro, Self-assembled dicopper(II) diethanolaminate cores for mild aerobic and peroxidative oxidation of alcohols, Dalton Trans 39 (2010) 9879–9888, doi:10.1039/C0DT00472C.
[105] A.M. Kirillov, P. Smolenski, Z. Ma, M.F.C. Guedes da Silva, M. Haukka, A.J.L. Pombeiro, Copper(I) iodide complexes derived from N-alkyl-1,3,5-triaza-7-phosphaadamantanes: synthesis, crystal structures, photoluminescence, and identification of the unprecedented $\{Cu_3I_5\}^{2-}$ cluster, Organometallics 28 (2009) 6425–6431, doi:10.1021/om900591q.
[106] A.W. Addison, T.N. Rao, J. Reedijk, J. Rijn, G.C. Verschoor, Synthesis, structure, and spectroscopic properties of copper(II) compounds containing nitrogen–sulphur donor ligands; the crystal and molecular structure of aqua[1,7-bis(*N*-methylbenzimidazol-2′-yl)-2,6-dithiaheptane]copper(II) perchlorate, J. Chem. Soc., Dalton Trans. 7 (1984) 1349–1356, doi:10.1039/DT9840001349.
[107] P. Pal, K. Das, A. Hossain, A. Frontera, S. Mukhopadhyay, Supramolecular and theoretical perspectives of 2,2′:6′,2′′-terpyridine based Ni(II) and Cu(II) complexes: on the importance of C–H$\cdots$Cl and $\pi\cdots\pi$ interactions, New J. Chem. 44 (2020) 7310–7318, doi:10.1039/D0NJ00094A.
[108] S. Das, G.P. Muthukumaragopal, S. Pal, S. Pal, A one-dimensional assembly of a square-planar copper(II) complex with alternating short and long Cu$\cdots$Cu distances. Metal ion spin-exchange *via* π-π interactions, New J. Chem. 27 (2003) 1102–1107, doi:10.1039/B212399C.
[109] M.N. Hoque, U. Manna, G. Das, Discrepancy in anion coordination directed by isomeric pyridine–urea receptors: solid state recognition of hydrated anions, Polyhedron 119 (2016) 307–316, doi:10.1016/j.poly.2016.09.022.
[110] M.N. Hoque, G. Das, Overview of the strategic approaches for the solid-state recognition of hydrated anions, CrystEngComm 19 (2017) 1343–1360, doi:10.1039/C6CE02438F.
[111] S.R. Choudhury, A.D. Jana, E. Colacio, H.M. Lee, G. Mostafa, S. Mukhopadhyay, Crowned tetrameric spirocyclic water chain: an unusual building block of a supramolecular metal–organic host, Cryst. Growth & Des. 7 (2007) 212–214, doi:10.1021/cg060837r.
[112] S. Pramanik, S. Konar, K. Chakraborty, T. Pal, S. Das, S. Chatterjee, M. Dolai, S. Pathak, Investigation of electrical conductance properties, non-covalent interactions and TDDFT calculation of a newly synthesized copper(II) metal complex, J. Mol. Struct. 1206 (2020) 127663–127670, doi:10.1016/j.molstruc.2019.127663.
[113] K.N.M. Daeffler, H.A. Lester, D.A. Dougherty, Functionally important aromatic–aromatic and sulfur–π interactions in the D2 dopamine receptor, J. Am. Chem. Soc. 134 (2012) 14890–14896, doi:10.1021/ja304560x.
[114] R.F.N. Silva, A.C.S. Sacco, I. Caracelli, J. Zukerman-Schpector, E.R.T. Tiekink, Sulfur(lone-pair)…π interactions with FAD in flavoenzymes, Z. Kristallogr. 233 (2018) 531–537, doi:10.1515/zkri-2018-2064.
[115] T.P. Tauer, M.E. Derrick, C.D. Sherrill, Estimates of the ab initio limit for sulfur–π interactions: the H_2S–benzene dimer, J. Phys. Chem. A 109 (2005) 191–196, doi:10.1021/jp046778e.
[116] Y.H. Peng, F.Y. Liao, C.T. Tseng, R. Kuppusamy, A.S. Li, C.H. Chen, Y.S. Fan, S.Y. Wang, M.H. Wu, C.C. Hsueh, J.Y. Chang, Unique sulfur–aromatic interactions contribute to the binding of potent imidazothiazole indoleamine 2,3-dioxygenase inhibitors, J. Med. Chem. 63 (4) (2020) 1642–1659, doi:10.1021/acs.jmedchem.9b01549.
[117] H. Nath, P. Sharma, R.M. Gomila, A. Frontera, M. Barcelo-Oliver, A.K. Verma, K. Dutta, M.K. Bhattacharyya, Unconventional enclathration of guest adipic acid and energetically significant antiparallel π-stacked ternary assemblies involving unusual regium-π(chelate) contacts in phenanthroline-based Ni(II) and Cu(II) compounds—Antiproliferative evaluation and theoretical studies, J. Mol. Struct. 1245 (2021) 131038, doi:10.1016/j.molstruc.2021.131038.
[118] A. Das, P. Sharma, A. Frontera, M. Barcelo-Oliver, A.K. Verma, R.S. Ahmed, S. Hussain, M.K. Bhattacharyya, Supramolecular assemblies involving biologically relevant antiparallel π-stacking and unconventional solvent driven structural topology in maleato and fumarato bridged Zn(II) coordination polymers: antiproliferative evaluation and theoretical studies, New J. Chem. 45 (2021) 13040–13055, doi:10.1039/D1NJ00619C.

[119] P. Sharma, H. Nath, A. Frontera, M. Barcelo-Oliver, A.K. Verma, S. Hussain, M.K. Bhattacharyya, Biologically relevant unusual cooperative assemblies and fascinating infinite crown-like supramolecular nitrate–water hosts involving guest complex cations in bipyridine and phenanthroline-based Cu(II) coordination compounds: antiproliferative evaluation and theoretical studies, New J. Chem. 45 (2021) 8269–8282, doi:10.1039/D1NJ01004B.
[120] J.C. Belmont-Sanchez, M.E. Garcia-Rubino, A. Frontera, J.M. Gonzalez-Perez, A. Castineiras, J. Niclos-Gutierrez, H-bonds, π-stacking and (water)O-H/π interactions in (μ_4-EDTA)bis(imidazole) dicopper(II) dihydrate, Crystals 11 (2021) 48, doi:10.3390/cryst11010048.
[121] M.K. Bhattacharyya, D. Dutta, S.M. Nashre-ul-Islam, A. Frontera, P. Sharma, A.K. Verma, A. Das, Energetically significant antiparallel π-stacking contacts in Co(II), Ni(II) and Cu(II) coordination compounds of pyridine-2,6-dicarboxylates: Antiproliferative evaluation and theoretical studies, Inorg. Chim. Acta 501 (2020) 119233, doi:10.1016/j.ica.2019.119233.
[122] M.N. Ahmed, M. Arif, F. Jabeen, H.A Khan, K.A. Yasin, M.N. Tahir, A. Franconetti A Frontera, On the importance of antiparallel π–π interactions in the solid state of isatin-based hydrazides, New J. Chem. 43 (2019) 8122–8131, doi:10.1039/C9NJ00405J.
[123] A. Najafi, M. Mirzaei, A. Bauza, J.T. Mague, A. Frontera, The roles of H-bonding, π-stacking, and antiparallel CO···CO interactions in the formation of a new Gd(III) coordination polymer based on pyridine-2,6-dicarboxylic acid, Inorg. Chem. Comm. 83 (2017) 24–26, doi:10.1016/j.inoche.2017.05.029.
[124] D. Debnath, S. Roy, A. Purkayastha, A. Bauza, R. Choudhury, R. Ganguly, A. Frontera, T.K. Misra, Synthesis and structure of 1,3-dimethyl-5-(*p*-sulfonamide-phenylazo)-6-aminouracil and its Ni(II) complex: topological insights and investigation for noncovalent interactions, J. Mol. Struct. 1141 (2017) 225–236, doi:10.1016/j.molstruc.2017.03.121.
[125] H. Andleeb, I. Khan, S. Hameed, A. Bauza, A. Frontera, M.N. Tahir, J. Simpson, A comparative experimental and theoretical investigation of hydrogen-bond, halogen-bond and π–π interactions in the solid-state supramolecular assembly of 2- and 4-formylphenyl arylsulfonates, ActaCryst C74 (2018) 816–829, doi:10.1107/S2053229618008355.
[126] J.D. Woodward, R.V. Backov, K.A. Abboud, D. Dai, H.-J. Koo, M.-H. Whangbo, M.W. Meisel, D.R. Talham, Dramatic variation of magnetic exchange through double end-on azide bridges in a series of ladder-like copper(II) coordination polymers, Inorg. Chem. 44 (2005) 638, doi:10.1021/ic049175q.
[127] J.-Y. Tsao, J.-D. Tsai, C.-I. Yang, Azide-bridged Cu(II), Mn(II) and Co(II) coordination polymers constructed with a bifunctional ligand of 6-(1*H*-tetrazol-5-yl)-2,2′-bipyridine, Dalton Trans. 45 (2016) 3388, doi:10.1039/C5DT04773K.
[128] J.-N. Li, Synthesis, characterization, and antibacterial activity of $[Cu_2(L^1)_3(NCS)]\cdot CH_3CN$ and $[Cu_2Br_2(L^2)_2(\mu_{1,1}\text{-}N_3)_2]$, Synth. React. Inorg., Met.-Org., Nano-Met. Chem. 43 (2013) 832, doi:10.1080/15533174.2012.750344.
[129] B.-L. Liu, N. Wu, C.-P. Li, J. Chen, Pseudohalide anion directed assemblies of two Cu^{II} complexes based on 3-(2-pyridyl)-4,5-bis(3-pyridyl)-1,2,4-triazole, Transition Met. Chem. 40 (2015) 341 http://dx.doi.org/10.1007%2Fs11243-015-9922-5.
[130] Y.-Y. Zhu, C. Cui, N. Li, B.-W. Wang, Z.-M. Wang, S. Gao, Constructing a series of azide-bridged Cu^{II} magnetic low-dimensional coordination polymers by using pybox ligands, Eur. J. Inorg. Chem. (2013) 3101–3111, doi:10.1002/ejic.201300107.
[131] E. Espinosa, E. Molins, C. Lecomte, Hydrogen bond strengths revealed by topological analyses of experimentally observed electron densities, Chem. Phys. Lett. 285 (1998) 170–173, doi:10.1016/S0009-2614(98)00036-0.